HHS Public Access

Author manuscript

Cancer Lett. Author manuscript; available in PMC 2022 August 28.

Published in final edited form as:

Cancer Lett. 2021 August 28; 514: 12–29. doi:10.1016/j.canlet.2021.05.006.

Disrupting interferon-alpha and NF-kappaB crosstalk suppresses IFITM1 expression attenuating triple-negative breast cancer progression

Olivia K. Provance[1], **Eric S. Geanes**[1], **Asona J. Lui**[1,2], **Anuradha Roy**[1,3], **Sean Holloran**[1,4], **Sumedha Gunewardena**[2], **Christy Hagan**[1,4,5], **Scott Weir**[1,5,6], **Joan Lewis-Wambi**[1,5,*]

[1]Department of Cancer Biology, University of Kansas Medical Center, Kansas City, KS 66160, USA

[2]Department of Molecular and Integrative Physiology, University of Kansas Medical Center Kansas City, KS 66160, USA

[3]High Throughput Screening Laboratory, University of Kansas, Lawrence, KS 66049, USA

[4]Department of Biochemistry, University of Kansas Medical Center Kansas City, KS 66160, USA

[5]The University of Kansas Cancer Center, Kansas City, KS 66160, USA

[6]The Institute for Advancing Medical Innovation, Kansas City, KS 66160, USA

Abstract

Overexpression of interferon induced transmembrane protein-1 (IFITM1) enhances tumor progression in multiple cancers, but its role in triple-negative breast cancer (TNBC) is unknown. Here, we explore the functional significance and regulation of IFITM1 in TNBC and strategies to target its expression. Immunohistochemistry staining of a tissue microarray demonstrates that IFITM1 is overexpressed in TNBC samples which is confirmed by TCGA analysis. Targeting

*Correspondence: jlewis-wambi@kumc.edu, Phone: 913-588-4739 Fax: 913-588-4701.

Author contributions

Conceptualization: Olivia Provance, Joan Lewis-Wambi
Methodology: Olivia Provance, Sean Holloran, Scott Weir, Anuradha Roy, Sumedha Gunewardena
Investigation: Olivia Provance, Eric Geanes, Asona Lui, Anuradha Roy
Validation: Olivia Provance, Eric Geanes
Formal Analysis: Olivia Provance, Asona Lui, Anuradha Roy, Sumedha Gunewardena
Visualization: Olivia Provance, Joan Lewis-Wambi
Writing (Original and Review): Olivia Provance, Joan Lewis-Wambi
Supervision: Joan Lewis-Wambi, Christy Hagan, Scott Weir
Project Administration: Joan Lewis-Wambi
Resources: All authors
Funding Acquisition: Joan Lewis-Wambi

CONFLICT OF INTEREST DISCLOSURE: None
The authors declare that they have no conflicts of interest to disclose.

Declaration of interests
☒ The authors declare that they have no known competing financial interests or personal relationships that could have appeared to influence the work reported in this paper.

IFITM1 by siRNA or CRISPR/Cas9 in TNBC cell lines significantly inhibits proliferation, colony formation, and wound healing *in vitro*. Orthotopic mammary fat pad and mammary intraductal studies reveal that loss of IFITM1 reduces TNBC tumor growth and invasion *in vivo*. RNA-seq analysis of IFITM1/KO cells reveals significant downregulation of several genes involved in proliferation, migration, and invasion and functional studies identified NF-κB as an important downstream target of IFITM1. Notably, siRNA knockdown of p65 reduces IFITM1 expression and a drug-repurposing screen of FDA approved compounds identified parthenolide, an NFκB inhibitor, as a cytotoxic agent for TNBC and an inhibitor of IFITM1 *in vitro* and *in vivo*. Overall, our findings suggest that targeting IFITM1 by suppressing interferon-alpha/NFκB signaling represents a novel therapeutic strategy for TNBC treatment.

Keywords

IFITM1; interferon; NF-kappaB; TNBC; parthenolide

1. Introduction

Approximately 12% of total breast cancer diagnoses are classified as triple-negative breast cancer (TNBC). These tumors lack the three most common receptors used for detecting and treating breast cancer: estrogen receptor (ER), progesterone receptor (PR), and the human epidermal growth factor receptor-2 (HER2) (1, 2). Patients diagnosed with TNBC have a 12-month median overall survival rate. This survival rate is significantly lower than patients diagnosed with ER+/PR+ breast cancer (56-month median survival) and HER2+ (20-month median survival) tumors (3–7). TNBC poor survival is attributed to the lack of molecular targets and a poor response to systemic chemotherapy (1, 8). Therefore, there is an urgent need to identify novel mechanisms promoting TNBC onset and progression to facilitate the development of more efficacious therapies.

TNBC is a highly heterogenous disease with multiple pathways implicated in its aggressive phenotype perhaps contributing to varied treatment response and survival outcomes (1). However, evidence suggests that unbalanced type I interferon (IFN) signaling influences TNBC patient survival and response to therapy (9–11). IFNs are cytokines that can be released by all cells in the body to inhibit viral infection, through upregulating interferon stimulated genes (ISG) as a mechanism of controlling cell death and survival pathways (12). Though both IFNα and IFNβ are classified as type I IFNs, previous studies suggest a specific role of IFNα in breast cancer biology (13–15). Canonically, IFNα activates JAK and TYK for phosphorylation of STAT1 and STAT2 and subsequent formation of the interferon stimulated gene factor-3 (ISGF3) complex consisting of pSTAT1, pSTAT2 and IRF9. Upon formation and nuclear translocation, ISGF3 induces ISG expression through binding to the interferon stimulated response elements (ISRE) in the promoter of ISGs. However, under chronic exposure to IFNα, the ISGF3 complex loses phosphorylation (U-ISGF3) but remains transcriptionally active, transcribing a specific subset of ISGs (16) which regulate cellular events including; apoptosis, senescence, migration or drug resistance (17). Additionally, IFN can also activate NFκB in a dose-dependent mechanism, and doing so, protects cells against apoptosis (18–20). Previous studies suggest crosstalk between

IFNα and NFκB such that the kinetics of IFN signaling and subsequent gene expression depend on concurrent NFκB activation, and vice versa, such that NFκB can regulate the IFN amplification loop (21). Supporting this evidence, multiple ISGs have NFκB binding sites within their promoter, but which ISGs are regulated by both IFNα and NFκB is highly context dependent (18, 22).

Interferon induced transmembrane protein-1 (IFITM1) is an ISG that is regulated by interferon signaling and NFκB activation (16, 23). IFITM1 is a 14-kDa membrane protein which was first described as a leukocyte antigen and a component of a membrane complex of tetraspanins responsible for regulating cell adhesion and proliferation (24). However, recent studies report that some tumors express elevated levels of IFITM1 compared to normal tissue (25–27) and that its overexpression correlates with drug resistance (13, 28–30) and tumor progression (25, 31, 32). Mechanistically, IFITM1 has been shown to enhance EGFR signaling (33), caveolin-1 activation (27), and regulate p21 nuclear translocation (13). Though IFITM1 has been identified as a tumor promoter in multiple types of cancer including endocrine resistant ER-positive breast cancers, its role in TNBC is unknown (13, 28). Therefore, elucidating the function and regulation of IFITM1 in TNBC can provide greater insight into its role in TNBC pathogenesis and possibly pave the way for its development as a novel therapeutic target.

In this study, we investigated the clinical and functional relevance of IFITM1 in TNBC and assessed the role of IFNα/NFκB signaling in regulating its expression. We found that IFITM1 is overexpressed in TNBC patient samples and TNBC cell lines and that genetic silencing of IFITM1 in TNBC cells reduces their ability to proliferate, migrate, and invade *in vitro* and *in vivo*. We further demonstrate that IFITM1 expression is regulated by enhanced IFNα and NFκB signaling which can be targeted by the naturally derived compound, parthenolide. Collectively, our data suggest that a subset of TNBC tumors overexpress IFITM1 and that targeting IFITM1 in these tumors might be therapeutically beneficial.

2. Materials and Methods

2.1 Cell lines and culture conditions

Human TNBC cell lines SUM149, MDA-MB-157, and MDA-MB-468 were used and were authenticated by STR allele profiling by Genetica DNA laboratories. SUM149 cells were obtained from Dr. Massimo Cristofanilli (Northwestern University, Chicago, IL, USA) who purchased them from Asterand Bioscience (Detroit, MI, USA). SUM149 cells were maintained in Ham's F-12 nutrient mixture (LifeTech) supplemented with 10% FBS (LifeTech), 5μg/mL insulin (Sigma), 1μg/mL hydrocortisone (Sigma), and 100 U/mL antibiotic-antimycotic (Sigma). MDA-MB-157 and MDA-MB-468 cells were obtained from Dr. Gustavo Miranda-Carboni (University of Tennessee Health Science Center). MDA-MB-157 and MDA-MB-468 cells were maintained in DMEM (LifeTech) supplemented with 20% FBS, 100 U/mL antibiotic-antimycotic and 1% glutamine (LifeTech). All cells were passaged twice weekly, with media changed every other day. All cells were cultured at 37°C in a 5% CO_2 atmosphere.

2.2 Clinical Samples

Clinical samples were provided by the KUMC Biospecimen Shared Resource as approved by KUMC IRB. A total of 34 primary TNBC breast tumors and 6 normal breast tissue samples from routine reduction mammoplasties were examined. Tissues were formalin-fixed with 10% neutral buffered formalin and paraffin-embedded (FFPE) prior to performing IHC. Clinicopathological data including age, race, clinical stage, HER2 staining and vascular invasion are shown in Table 1. After review of the hematoxylin and eosin slides and marking of tumor areas, 2-mm tissue cores of representative tumor areas were extracted and inserted in recipient blocks. IHC analysis for IFITM1 was then performed on these samples (See IHC staining protocol below). Two cores from each tumor were analyzed to account for the impact of tumor heterogeneity on IFITM1 expression. IFITM1 staining intensity was quantified manually on a scale of 0–3 where 0 means no staining, 1+ is faint staining (light brown), 2+ is moderate staining (yellowish brown) and 3+ is strong staining (brown). Cores were scored by three independent individuals including a senior pathologist at KUMC. Any discrepancies were resolved by group consensus. Final distribution of IFITM1 expression is shown in Table 2.

2.3 Immunohistochemistry (IHC), immunofluorescence (IF) and TUNEL staining of human and mouse tumors

IHC staining was performed after tissue deparaffinization by clearance in xylene and hydration through graded ethanol series. Antigen retrieval was conducted at 99°C in Dako Target retrieval solution for 20 min per manufacturer's instructions (Agilent Technologies: #S1700). For human samples, blocking was performed using 5% normal horse serum and antibody dilution was performed in 0.01% Triton-X. Sections were stained using primary human antibodies targeted against IFITM1(Santa Cruz: sc-374026) and biotinylated secondary antibodies (Vector Labs). Immunoperoxidase signal was produced using 3,3′-Diaminobenzidine (DAB) and amplified using the Vectastain® Elite ABC Kit (Vector Laboratories). Sections were stained using human antibodies for anti-Ki67 (Dako: #M7240), anti-IFITM1 (Santa Cruz: sc-374026), anti-phospho-p65 (Cell Signaling Technologies: #3033S) and anti p-65 (Cell Signaling Technologies: #8242) or anti-smooth muscle actin (Spring Biosciences #E2464). Tissue sections were counter stained using hematoxylin and mounted in xylene. Slides were imaged on a Nikon Eclipse 80i Upright Microscope in the KUMC imaging core.

IF staining of mouse tumors was performed after tissue deparaffinization by clearance in xylene and hydration through graded ethanol series followed by antigen retrieval as described above. IF method has been described previously (13). Due to the use of mouse antibodies on mouse tissue, blocking and antibody dilution were performed using the Mouse on Mouse (MOM™) kit per manufacturer's instructions (Vector Labs: BMK-2202). Sections were stained using human antibodies for anti-Keratin 19 (Neomarkers: #MS-198-P1) or anti-smooth muscle actin (Spring Biosciences: #E2464). Secondary antibodies were FITC (Vector Laboratories: FI-1000) or Texas Red conjugated (Santa Cruz: sc-362277). ProLong® Gold Antifade Reagent with DAPI (Cell Signaling: P36935) was used to stain the nuclei and mount the slides. Slides were visualized on a Leica TCS SPE confocal microscope in the Confocal Imaging Core at the University of Kansas Medical Center.

Images were collected and analyzed using the Leica LAS AF Lite software (Leica Biosystems).

TUNEL staining was performed using the Click-iT™ Plus TUNEL assay kit (Thermo Fisher: #C10617) on deparaffinized tissue or methanol fixed cell lines grown on chamber slides following the manufacturer's instructions. The average number of TUNEL positive cells was quantified using the binary transformation and cell counting method in ImageJ.

2.4 Western blotting and co-immunoprecipitation

Cells were seeded in 6-well plates or 10cm culture dishes and collected using a cell scraper and lysed in RIPA buffer (Thermo Scientific, Cat. #89901) supplemented with protease inhibitor cocktail (Roche Diagnostics, Cat. #11836–153–001) and phosphatase inhibitor (Sigma, Cat. #P0044). Cells were homogenized over ice by sonication and purified by centrifugation. Protein concentration was determined by Bio-Rad protein assay (Biorad: Cat. #5000006). Proteins were separated by 4–12% SDS–polyacrylamide gel electrophoresis (NuPage, Cat. #NP0335 and #NP0336) and electrically transferred to a polyvinylidene difluoride membrane. After blocking the membrane using non-fat milk or BSA target proteins were detected using anti-IFITM1 (1:200, SantaCruz: sc-374026), anti-IRF9 (1:200, SantaCruz: sc-365893), anti-STAT2 (1:200, SantaCruz: sc-1668), anti-STAT1 (1:200, SantaCruz: sc-464) or anti-phospho-p65 (1:500, Cell Signaling Technologies: #3033S) and anti p-65 (1:500, Cell Signaling Technologies: #8242). Membranes were stripped and re-probed for β-actin (1:15,000, Cell Signaling Technologies: #3700). The appropriate horseradish peroxidase (HRP)-conjugated secondary antibody (Cell Signaling Technologies: Mouse #7076, Rabbit #7074) was applied and the positive bands were detected using Amersham ECL Plus Western blotting detection reagents (GE Health Care: RPN2106) or Immobilon® Crecendo Western HRP Substrate (MilliporeSigma: WBLUR0500) and exposed to autoradiography film (Midwest Scientific).

For co-immunoprecipitation experiments, cell lysates were collected in RIPA buffer (150mM NaCl, 6mM disodium phosphate, 4mM monosodium phosphate, 2mM EDTA pH=8, 1% Triton-X 100, 50mM sodium fluoride) supplemented with supplemented with protease inhibitor cocktail (Roche Diagnostics, Cat#11836–153–001) and phosphatase inhibitor (Sigma, Cat#P0044). Cell lysates containing at least 1000μg/mL concentrations were incubated overnight at 4°C with 5μL of anti-rabbit-IRF9 antibody (Cell Signaling Technology: #76684S) or 1μL of rabbit IgG per reaction. Protein A coated magnetic beads (Invitrogen: #10001D) were washed with supplemented RIPA and added in a final volume of 100μL and followed by an incubation time of 2 hours. Immune complexes were washed three times with PBS, resuspended in Laemelli sample buffer containing dithiothreitol and β-mercaptoethanol (Invitrogen, Cat#NP0007), boiled for 5 minutes, and subjected to western blotting.

2.5 Small interfering RNA (siRNA) transfections

SUM149, MDA-MB-468 and MDA-MB-157 cells were seeded overnight and transfected at 60–80% confluency with 60–100nM of targeted siRNAs or scrambled RNA (siControl Santa Cruz Biotechnology: sc-37007) introduced by Lipofectamine 2000™ (Invitrogen:

#1668019) in OptiMEM Reduced-Serum Medium (Gibco: #11058–021). After overnight incubation the transfection mixture was replaced with normal culture medium. MDA-MB-468, MDA-MB-157 and SUM149 cells were transfected with pooled siRNA's targeting STAT1 (Santa Cruz Biotechnology: sc-44123), STAT2 (Santa Cruz Biotechnology: sc-29492) and IRF9 (Santa Cruz Biotechnology: sc-38013) and harvested 48 hours post transfection for western blot analysis. MDA-MB-468 and MDA-MB-157 cells were transfected with pooled small-interfering RNAs (siRNAs) targeting IFITM1 (Santa Cruz Biotechnology: sc-44549) which has been validated previously (14). siCon and siIFITM1 cells were then used for functional *in vitro* assays as described below in section 2.8.

2.6 CRISPR/Cas9-Mediated Gene Knockout

SUM149 and MDA-MB-157 cells were subjected to CRISPR/Cas9-mediated knockout of IFITM1 by lentiviral transduction using particles from OriGene™ Technologies (Catalog number: KN201617). The guide RNA vector 5'- TGATCACGGTGGACCTTGGA-3' or a scrambled control was cloned into a pCas-Guide vector which expresses Cas9 behind CMV and U6 promoters. This vector was co-transfected with the donor template including homologous arms and a functional GFP-puromycin cassette using Turbofectin 8.0 (Origene: #TF81001) as the delivery reagent. For SUM149, cells were passaged at a 1:10 ratio 48 hours post-transfection for 8 passages. Cells were treated with 1000μg/mL puromycin daily. Single cells were grown in puromycin until colonies formed. Both clonal populations and a pooled population of all puromycin resistant cells were expanded and screened for absence of IFITM1 protein expression using the IFITM1 antibody. The pooled population of CAS9/Control cells and IFITM1 KO cells were then used for functional *in vitro* assays as described below in section 2.8. For MDA-MB-157, transfected cells were passaged at a 1:2 ratio for 8 passages prior to treatment with 250–350μg/mL puromycin for one week.

2.7 High Throughput Drug Screen

The drug repurposing collection at KUCC contains 3,574 FDA-approved and abandoned drugs from the following vendors: Selleck (1288), Enzo (640), NIH (446) and Prestwick (1,200). The drugs are stored at 10 mM in 100% dimethyl sulfoxide (DMSO). KUCC maintains and continues to grow an internal, integrated database describing activities (and, lack thereof) of FDA-approved and abandoned drugs evaluated in high throughput screens across many proposed drug targets employing cell-based and biochemical assays. For the screen, SUM149 and MDA-MB-157 (1000 cells/well) plated in 384-well microplates. The drugs and DMSO controls were added to the plates using Echo 555 (Labcyte Inc.) at a final concentration of 2.5μM. After 72 hours incubation at 37°C, cytotoxicity was measured using the luminescence-based CellTiter-Glo reagent (Promega Inc.). The luminescence was read on Enspire plate reader (PerkinElmer Inc.) and percent cytotoxicity was normalized to positive and negative controls on each assay plate. The Z' scores of the two repurposing screens were: (A) SUM149 screen, average Z'= 0.91 ± 0.018, (B) MDA-MB157 screen, average Z'= 0.81 ± 0.034, indicating a good separation of positive and negative controls across all assay plates and suitability of the assay for compound screening. In addition to the assay performance criteria described above, cytotoxicity was defined as drugs demonstrating greater than 50% inhibition of cell viability in one or both breast cancer cell lines screened

with no observed toxicity in normal cells. Parthenolide was one of the compounds identified for further *in vitro* analyses.

2.8 Proliferation, colony formation, and wound healing assays

Cell proliferation was measured by cell counting. Cells were seeded onto a 24-well plate at a density of 25,000 cells/well. The next day, cells were either transfected, treated, or harvested for the 0-hour timepoint. Cells were counted every 24 hours and the final values were normalized to the 0-hour timepoint or to DMSO. Cells were re-treated with parthenolide at the IC50 or with equivalent concentrations of DMSO every 48 hours when indicated.

For colony formation, cells were seeded onto a 6-well plate at 1,000 cells/well. For experiments using parthenolide, cells were treated 24 hours after plating and re-treated every 48 hours. For all experiments cells were grown for 8–14 days prior to staining colonies with 5% crystal violet and imaged using the ChemiDoc™ XRS system equipped with Image Lab™ software.

Wound healing was assessed by seeding cells onto a 24-well plate at a density of 90,000–120,000 cells/well (approximately 80% confluency) and making a single wound by scratching the attached cells using a 10-μl sterile pipette tip. The plates were washed with complete medium to remove cellular debris. Images of the cells were taken immediately after and 24, 48, and 72 hours later using a phase-contrast microscope and wound area was quantified using the Wound Healing Tool in ImageJ. Cells were re-treated with parthenolide at the IC50 every 24 hours when indicated.

2.9 Animal Experiments

Recipients were 7–10-week-old virgin female NOD-SCID IL2Rgamma^{null} (NSG) mice which were purchased from Jackson Laboratories. Animal experiments were conducted following protocols approved by the University of Kansas School of Medicine Animal Care and Use (ACUP#: 2016–2341 and 2020–2596-02). Mice were maintained in the animal facility at KUMC under specific-pathogen free conditions.

To assess tumor growth, the orthotopic fat pad model was used. For this experiment, mice were randomly divided into two groups. Each mouse was inoculated with SUM149 CAS9/Control cells or IFITM1 KO cells suspended in 50:50 PBS/Matrigel (Corning) through bilateral injection into the 4th mammary fat pads as described previously (34). Briefly, 3 × 10^6 cells were delivered per injection in a volume of 100μL. The length (L) and width (W) of tumors was measured weekly with digital calipers, and the tumor volume was calculated by the formula $W^2/(2L)$. Tumors grew for 26 days after seeding and then the mice were sacrificed, and tumors excised, measured, and weighed. Solid tumors were fixed in 10% formalin (4% formaldehyde solution; Fisher SF98–4) prior to processing and staining.

To assess tumor cell invasion, the mammary intraductal (MIND) model was used as previously described (35). Briefly, SUM149 CAS9/Control cells or IFITM1 KO cells were resuspended as single cells in PBS and counted. A 30-gauge Hamilton syringe, 50-μl capacity, with a blunt-ended 1/2-inch needle was used to deliver the cells. The mice were anesthetized by ketamine/xylene injection and a Y-incision was made on the abdomen

allowing exposure of the inguinal mammary fat pads. The nipple of the inguinal gland was snipped for direct needle insertion. Two microliters of cell-culture medium (with 0.1% trypan blue) containing 2,500 to 5,000 cells/μl were injected. Successful injection was confirmed by visual detection of trypan blue in the ductal tree branches. The skin flaps were then repositioned normally and held together with wound clips. After 6 weeks mice were sacrificed mammary glands were excised and weighed. Mammary glands were fixed in 10% formalin (4% formaldehyde solution, Fisher SF98–4) prior to processing and staining.

To assess the *in vivo* effect of parthenolide in TNBC, the orthotopic fat pad model was used. Parthenolide was obtained from Cayman Chemicals (#70080). 7-week old female NSG mice were divided randomly into four groups: SUM149 IFITM1+ 10% DMSO, SUM149 IFITM1+ 30mg/kg/day parthenolide, MDA-MB-468 IFITM1+ 10% DMSO, and MDA-MB-468 IFITM1+ 30mg/kg/day parthenolide. 3×10^6 cells suspended in PBS were injected bilaterally into the fourth mammary fat pad of NSG mice. When tumors reached a mean volume of $150mm^3$, mice were treated with 30mg/kg/day parthenolide or with equivalent volume of 10% DMSO through intraperitoneal injections for 14 to 21 days. Mice were weighed weekly and tumors were measured every 48 hours. At the conclusion of the experiment, mice were euthanized, and tumors were excised, measured, weighed, and then fixed in 10% formalin (4% formaldehyde solution, Fisher SF98–4) for IHC staining. For western blotting, unfixed tumors were homogenized with a tissue tearer and cell lysates were assessed as discussed above.

2.10 RNA Sequencing and Functional Transcriptomic Analysis

RNA-Sequencing was performed at a strand specific 100 cycle paired-end resolution, in an Illumina NovaSeq 6000 sequencing machine (Illumina, San Diego, CA). The CAS9/Control and the IFITM1 KO pooled samples were analyzed in triplicate. The initial read quality was assessed using the FastQC software (36). The average per sequence quality score measured in the Phred quality scale was above 30. Reads were mapped to the human genome (GRCh38) using the STAR software, version 2.3.1z. On average, 99% of the sequenced reads mapped to the genome, resulting in 30 to 42 million mapped reads per sample, of which on average 95.5% were uniquely mapped reads. Differential gene expression analysis was performed using the Cuffdiff software, version 2.1.1. The number of transcripts mapped to each gene was quantified using the RSEM software. Expression normalization and differential gene expression calculations were performed in edgeR to identify statistically significant differentially expressed genes. The resulting p-values were adjusted for multiple hypothesis testing using the Benjamini and Hochberg method (37).

Genes that were up- or downregulated by at least 2-fold (P 0.05, FDR0.05) and had a FPKM (Fragments per kilo base per million mapped reads) value of ≥ 1 when comparing IFITM1 KO cells to CAS9/Control provided 561 analysis ready molecules. Ingenuity pathway analysis (IPA) was performed using the ingenuity pathway analysis software (QIAGEN). Pathways were identified through the diseases and biological function analysis on IPA. The activation z-score was calculated to infer activation states of upstream regulators.

2.11 Clinical Analyses

The UALCAN resource was used to assess expression of IFITM1 in TNBC compared to normal breast from the TCGA database and the expression of IFITM1 in HER2neg metastatic breast cancer (38). Relapse free survival data were obtained from the 2020 version of the Kaplan-Meier Plotter breast cancer survival database (http://kmplot.com/analysis/index.php?p=service&cancer=breast) (39). The 143 breast cancer patient samples used in the analysis were obtained by first delineating basal subtype and further by the Pietenpol mesenchymal subtype. Patients were stratified by IFITM1 expression (probe set 214022_s_at) relative to the upper and lower quartiles (107 patients in upper quartile, and 36 patients in lower quartile). The p-value was calculated using a log-rank test. IFITM1 gene expression in invasive primary breast cancer compared to normal breast tissue was analyzed using the Oncomine™ platform (40, 41). IFITM1 gene expression stratified by grade and nodal status and correlation with genes in the NFκB pathway was analyzed using bcGenExMiner (42).

2.12 RNA isolation and RT-PCR analysis

Total RNA was isolated from cultured cells using a QIAGEN RNeasy Mini Kit Qiagen (Cat #74104) according to the manufacturer's protocol. First strand cDNA synthesis was performed from 3 μg total RNA using MulV Reverse Transcriptase (Invitrogen: Cat. #28025–013), RNAse inhibitor (Applied Biosystems: Cat. #N8080119), random hexamers (Invitrogen: Cat. #100026484), deoxynucleotide triphosphates and colorless PCR buffer (Promega: Cat. #M792A) on a Bio Rad MyCycler™. RT-PCR was conducted using the ViiA™ 7 Real-Time PCR system (Applied Biosystems) and SYBR Green Reagent (Life Technologies: #4367659) with 25 pmol primers obtained from Integrated DNA Technologies. Specific human sequences listed in Table 3. Relative mRNA expression level was determined as the ratio of the signal intensity to that of PUM1 using the formula: $2^{-\Delta CT}$. For experimental comparisons, fold change in expression was normalized to PUM1 and then compared to control for that experiment using the formula: $2^{-\Delta\Delta CT}$.

2.13 Luciferase assays

For NFκB promoter assay, 0.8 μg of plasmid DNA pGL4.32 NFκB-RE vector (Promega) containing 5x NFκB-RE was co-transfected with the pRL CMV Renilla vector. The NFκB plasmid was a kind gift from Dr. Christy Hagan (University of Kansas Medical Center). After 24 hours, transfection reagent was replaced with normal cell culture media containing parthenolide or IFNα where indicated. Luciferase and Renilla activities were measured 24 hours later using the Dual-Luciferase® reporter assay kit (Promega: E1910) according to the manufacturer's instructions on a BioTek Synergy 4 microplate reader using the Gen 5 data analysis software.

3. Results

3.1 Clinical relevance of IFITM1 in triple-negative breast cancer

To define the clinical relevance of IFITM1 in TNBC, we first stained 34 primary TNBC breast tumor samples and 6 normal breast tissue samples through immunohistochemistry

(IHC) for IFITM1 expression (Fig. 1A). We found that 0% (0/6) normal breast tissue samples had IFITM1 while 38% of TNBC breast tumors overexpressed IFITM1 as measured by a staining intensity of 2+ and 62% of TNBC breast tumors had 1+ intensity. To expand our analysis to a larger patient cohort, we analyzed TCGA data and found that IFITM1 is significantly elevated in TNBC patient samples compared to normal breast tissue (Fig. 1B). Moreover, utilizing the Kaplan-Meier Plotter breast cancer survival database we found that IFITM1 expression correlates with decreased relapse free survival for patients with mesenchymal TNBC and is elevated in invasive breast tumors and those with higher grade and nodal positivity, and metastasis (Fig. 1C, Supplemental Fig. S1) (39). For comparison, we assessed IFITM1 expression in several breast cancer cell lines. We found that IFITM1 protein is highly expressed in SUM149, MDA-MB-157 an MDA-MB-468 TNBC cells, but not expressed in estrogen receptor (ER) positive MCF-7 and T47D breast cancer cell lines, or the normal, immortalized ER-negative MCF10a cells (Fig. 1D). Lastly, qRT-PCR analysis confirms higher expression of IFITM1 mRNA in TNBC cells compared with ER+ MCF-7 cells (Fig. 1E).

3.2 Loss of IFITM1 decreases TNBC proliferation, colony formation and wound healing *in vitro*

To investigate the functional significance of IFITM1 expression in TNBC, CRISPR/Cas9 was used to create stable IFITM1 KO SUM149 and MDA-MB-157 cell lines (Fig. 2A). We found that both SUM149 IFITM1 KO cells and MDA-MB-157 IFITM1 KO cells have a slower growth rate than their CAS9/Control counterparts as assessed by cell counting (Fig. 2C) and that the IFITM1 KO cells have a significantly impaired ability to form colonies (Fig. 2D,E) and to migrate after 24 and 48 hours (Fig. 2F,G). Furthermore, this data is supplemented with the use of siRNA against IFITM1 in MDA-MB-157 and MDA-MB-468 cells (Supplemental Fig. S2A). We found that loss of IFITM1 significantly inhibits cell growth in MDA-MB-157 and MDA-MB-468 cells (Supplemental Fig. S2B–C) and cell migration in MDA-MB-157 cells (Supplemental Fig. S2D) but not in MDA-MB-468 cells (Supplemental Fig. S2E). Overall, these data confirm that the presence of IFITM1 in SUM149, MDA-MB-157 and MDA-MB-468 cells supports their growth and migration *in vitro*.

3.3 Loss of IFITM1 inhibits SUM149 tumor growth and invasion *in vivo*

As a proof of concept to determine if loss of IFITM1 has the same impact *in vivo*, we assessed tumor growth via the orthotopic fat pad model using NSG mice. SUM149 CRISPR edited cells were used in this experiment due to the permanent decrease of IFITM1 expression and ability to grow *in vivo.* Tumors were developed by inoculating the mammary fat-pad of female mice with either SUM149 CAS9/Control or SUM149 IFITM1 KO cell lines. We found that loss of IFITM1 statistically significantly reduces SUM149 tumor volume from 350mm^3 (Cas9/control) to 50mm^3 (IFITM1 KO) and SUM149 tumor weight from 420mg (Cas9/control) to 100mg (IFITM1 KO) (Fig. 3A–C, Supplemental Fig. S3 A) at day 26. A decrease in Ki67 staining (Fig. 3D) and an increase in TUNEL staining (Fig. 3D) demonstrate that the decrease in tumor growth is a result of decreased proliferation and increased cell death. These data suggest that IFITM1 enhances SUM149 TNBC tumor growth *in vivo* and its loss inhibits growth through cell death.

Since the loss of IFITM1 significantly inhibits migration (Fig. 2) and clinical data suggest IFITM1 is elevated in invasive breast tumors (Supplemental Fig. S1), we utilized the mammary intraductal (MIND) model to assess the effect of IFITM1 knockout on local SUM149 tumor cell invasion *in vivo* (Fig. 3E). In the MIND model, breast cancer cells are injected into the mammary duct through the nipple, where they populate the duct and can invade into the surrounding mammary gland (35). IHC for IFITM1 and smooth muscle actin (SMA; milk duct marker) (Fig. 3F) and H&E staining (Supplemental Fig. S3 B), allowed visualization of IFITM1 expression, mammary gland architecture, and the extent of tumor invasion to quantify the total number of lesions and number of invasive lesions per field (Fig. 3G). Immunofluorescence of SMA (shown in green) and human keratin-19 (human breast cancer cell marker; shown in red) (Fig. 3F) was used to assess the average invasion distance outside the duct (Fig. 3G). Together, these data demonstrate that loss of IFITM1 decreases the ability of SUM149 tumor cells to invade out of the mammary duct and into the stroma.

3.5 RNA sequencing identifies signaling pathways affected by loss of IFITM1

To assess the mechanism whereby loss of IFITM1 decreases TNBC growth and invasion, RNA sequencing was performed on SUM149 CAS9/Con and IFITM1 KO cells. We identified that 1, 358 genes were significantly differentially regulated in IFITM1 KO cells compared to CAS9/Control cells with a p-value of 0.05, a false discovery rate of 0.05, a fold-change threshold of 2.0 (Fig. 4A). Stringency was enhanced by ensuring FPKM (fragments per kilobase per million) were ≥ 1 which provided 561 differentially regulated genes. Of those genes, the IFITM1 KO cells had 294 upregulated and 267 downregulated genes compared to CAS9/Control (Supplemental Fig. S4). Analysis of the 267 genes downregulated in the IFITM1 KO cells compared to CAS9/Con cells using Ingenuity Pathway Analysis (IPA) identified a negative Z-score (suggestive of downregulation or inhibition) for pathways of proliferation, migration, and invasion (Fig. 4B, Supplemental Fig. S4), corroborating both *in vitro* and *in vivo* data. Using the upstream analysis tool in IPA we identified the NFκB pathway to be significantly downregulated in IFITM1 KO cells compared to CAS9/Control cells (Fig. 4C). Particularly, multiple NFκB related genes including RELA (p65), NFKB1 (p105), NFKB2 (p100), cREL, and IkBα are downregulated (Fig. 4C). To visualize NFκB gene regulation, we overlaid IFITM1 KO versus CAS9/Con fold change-values to genes regulated by the NFκB complex as grouped by IPA. Fig. 4D depicts the genes in which their downregulation is mediated by loss of IFITM1 through the NFκB complex. Solid lines represent direct regulation and dash lines represent indirect regulation. These results were validated through qRT-PCR as loss of IFITM1 significantly decreases the mRNA expression of RELA (p65), NFKB1 (p105), NFKB2 (p100), and key NFκB target genes (IL6 and SNAI2) involved in growth and invasion (Fig. 4E). Additionally, correlation between IFITM1 and factors of the NFκB signaling pathway shows a slight positive trend when assessing publicly available clinical RNA sequencing data (Fig. 4F). Collectively, these results suggest that loss of IFITM1 decreases NFκB complex transcriptional activity and subsequent gene expression in SUM149 cells.

3.6 IFNα and NFκB signaling regulate IFITM1 expression in TNBC

We have previously demonstrated that IFITM1 is regulated by IFNα, however, luciferase assay using IFITM1 deletion mutants suggests that NFκB may also play a role in regulating

IFITM1 expression (13). To gain a better insight into whether NFκB directly regulates IFITM1 expression in TNBC cells we utilized siRNA to decrease p65 expression. Reduction of levels in all three TNBC cell lines significantly inhibits IFITM1 protein (Fig. 5A) and mRNA expression (Fig. 5B). Since IFNα regulates IFITM1 expression (14) and can regulate NFκB activation (18, 20) we assessed whether autocrine IFNα signaling through the IFNAR receptor impacts NFκB activation. TNBC cells were treated with 5μg/mL of IFNAR2 neutralizing antibody for 24 hours resulting in a reduction of IFITM1 in all three cell lines (Fig. 5C) and a trend of decreased phosphorylation of p65 (Fig. 5C, D). Regarding IFN signaling, we confirmed that STAT2 and IRF9, key components of the ISGF3 complex, are also important in regulating IFITM1 expression since loss of STAT2 and IRF9, but not STAT1, reduces IFITM1 expression in the TNBC cell lines (Fig. 5E). Notably, we observed that the TNBC cell lines expressed very low to undetectable basal levels of pSTAT2 (Fig. 5F), however, STAT2 was still able to bind to IRF9 (Fig. 5G), thus suggesting a role for an unphosphorylated ISGF3-like complex in regulating IFITM1 expression. Collectively, these data suggest that IFITM1 is regulated by both IFNα and NFκB signaling pathways.

3.7 Drug repurposing identifies parthenolide as an agent to inhibit TNBC cell growth and migration and IFITM1 expression

Since our data suggest IFITM1 is an important mediator of TNBC growth, migration, and invasion, a high-throughput screen of FDA-approved drugs was used to identify agents with the potential to target IFITM1 expression. Our initial screen identified parthenolide, a naturally derived NFκB inhibitor, as a potent growth inhibitor in SUM149 cells. We then confirmed activity by generating concentration-response curves of parthenolide in four TNBC breast cancer cell lines (SUM149, MDA-MB-468, MDA-MB-157 and MDA-MB-231). As results are depicted in Fig. 6A and Supplemental Table 1, SUM149 has the lowest IC50 (4.1μM) followed by MDA-MB-468 (4.5μM), and MDA-MB-157 (6.8μM), while MDA-MB-231 cells, which lack IFITM1, have the highest IC50 (15.8μM).

Next, SUM149, MDA-MB-468, and MDA-MB-157 cell lines were treated with parthenolide at the IC50 and assessed for cellular clonogenicity, proliferation, wound healing, and apoptosis. We found that parthenolide significantly inhibits TNBC colony formation (Fig. 6B, Supplemental Fig. S5A–C), proliferation (Fig. 6C), and wound healing (Supplemental Fig. S5D). Lastly, parthenolide induces PARP cleavage and increased TUNEL staining which are important markers of apoptosis (Supplemental Fig. S6).

Next, we assessed whether parthenolide can regulate IFITM1 expression. We found that parthenolide inhibits p65 activation in SUM149, MDA-MB-157 and MDA-MB-468 cells (Fig. 6D) and it significantly reduces NFκB promoter activity in SUM149 cells (Fig. 6E). Notably, parthenolide significantly inhibits IFITM1 protein (Fig. 6F) and mRNA expression (Fig. 6G) in all cell lines. Interestingly, we found that parthenolide also significantly inhibits IFNα mRNA levels in SUM149 cells (Fig. 6H) and that exogenous IFNα followed by treatment with parthenolide does not rescue the IFITM1 expression in SUM149, MDA-MB-468 or MDA-MB-157 cells (Fig. 6I).

3.8: In vivo effects of parthenolide

To assess the effect of parthenolide *in vivo*, the orthotopic fat pad model was used. Tumors were developed through bilateral injection of SUM149 or MDA-MB-468 cell lines into the mammary fat-pads of 7-week old female NSG mice. Mice were treated intraperitoneally with a 10% DMSO solution or 30mg/kg/day parthenolide for 14–21 days. Parthenolide treatment significantly decreased MDA-MB-468 tumor volume from 500mm^3 to 200mm^3 and tumor weight from 175mg to 130mg after 14 days of treatment (Fig. 7A–B). An increase in apoptosis as measured by TUNEL staining (Fig. 7C) and a decrease in Ki67 staining (Fig. 7D) suggests parthenolide reduces proliferation and induces cell death *in vivo*. Moreover, IHC analysis suggests that this is due to a decrease in phospho-p65 and IFITM1 expression (Fig. 7D). Similarly, parthenolide significantly reduces SUM149 tumor volume from 1,200mm^3 to 550mm^3 (Fig. 7E) and tumor weight from 900mg to 400mg (Fig. 7F) after 21 days of treatment and slightly decreases IFITM1 and the ratio of phospho-p65 to p65 (Fig. 7G). We should note that there were no adverse effects or potential toxicity associated with parthenolide treatment as demonstrated by no significant body weight loss in the mice (Supplemental Figure S7). These data suggest that parthenolide has a similar effect *in vivo* as it does *in vitro*.

3.9: IFITM1 is an indirect target of parthenolide

To determine whether parthenolide inhibits tumor cell growth through direct targeting of IFITM1, we assessed the effect of parthenolide in SUM149 and MDA-MB-157 CRISPR/Con and IFITM1 KO cells. We found that loss of IFITM1 in SUM149 cells (Fig. 8A) and in MDA-MB-157 cells (Fig. 8B) significantly enhances sensitivity to parthenolide when treated with both half the IC50 and the full IC50 values at 72-hours as assessed by cell growth. This data is further supported by 2D colony formation which shows that loss of IFITM1 significantly reduces colony formation upon fractionated doses of parthenolide treatment in both SUM149 cells (Fig. 8D–E) and in MDA-MB-157 cells (Fig. 8F). The fact that TNBC cells retain their sensitivity to parthenolide despite their loss of endogenous IFITM1 suggests that parthenolide may not directly target IFITM1, but rather, targets the upstream regulators of IFITM1: NFκB and IFNα, as depicted in our schematic overview shown in Fig. 9.

4. Discussion

Triple negative breast cancer (TNBC) is the most aggressive subtype of breast cancer and the absence of well characterized, druggable targets and disease heterogeneity provide significant therapeutic barriers (8). The interferon stimulated gene, IFITM1 has been shown to enhance tumor growth, migration, and invasion in head and neck, gastric, and colorectal cancers (25, 26, 32). Though our lab has previously identified an important role for IFITM1 in aromatase inhibitor resistant breast cancer (13), the role of IFITM1 in TNBC was unknown. In the present study we show for the first time that IFITM1 is overexpressed in a subset of TNBC patient samples and cell lines compared to normal breast tissue and ER+ breast cancers. Generation and characterization of two IFITM1-null TNBC cell lines (SUM149 and MDA-MB-157) with CRISPR/Cas9 gene editing allowed investigation into the functional role of IFITM1 in TNBC both *in vitro* and *in vivo*. Functional studies

demonstrate that IFITM1 promotes TNBC growth, colony formation, migration, and invasion which may be attributed to the decrease of NFκB signaling. Importantly, we discovered that the naturally derived NFκB inhibitor, parthenolide, inhibits both IFNα and NFκB pathways, subsequently inhibiting IFITM1 expression, decreasing TNBC growth, and inducing TNBC cell death both *in vitro* and *in vivo.* Overall, these findings are twofold such that they suggest IFITM1 regulates TNBC growth, migration, and invasion, and that targeting both IFNα and NFκB signaling with parthenolide might be a novel therapeutic strategy for a subset of TNBC that overexpress IFITM1.

Our present finding that IFITM1 mediates TNBC progression aligns with previous reports in numerous cancer subtypes (13, 25, 26, 32). While the mechanism whereby IFITM1 regulates these phenotypes is unclear, we observe that IFITM1 regulates NFκB signaling as observed through RNA sequencing which is a key regulator of growth and invasion in breast cancer (43, 44). IFITM1 has also been shown to enhance EGFR signaling (33) and caveolin-1 activation (27) in some tumors. Importantly, studies in virology provide additional insight into how IFITM1 functions. IFITM1 inhibits viral infection at the plasma membrane through interaction with multiple tetraspanin family members including CD81 (45), a tumor promoter in TNBC, that regulates integrins and phosphoinositide signaling (46, 47). In a THP-1 model, IFITM1 mediates ERK and PI3K signaling, thus increasing MMP9 expression (48), and in letrozole resistant breast cancer, IFITM1 contributes to activation of AKT signaling (29). Though this is the first study to suggest a role of IFITM1 on NFκB signaling, these previous studies indirectly support our findings since ERK, AKT, and PI3K signaling have been identified to regulate NFκB activation through non-canonical mechanisms (48). Perhaps loss of IFITM1 results in perturbation of membrane microdomains which are home to many receptors, kinases, and co-factors thus inhibiting these downstream signaling pathways (30). Another important observation regarding IFITM1 is that it is expressed in the both the stromal and tumor cells (Fig. 1). Though is well known that the stroma plays an important role in facilitating response to therapies and tumor progression, there is limited data regarding the function of IFITM1 expression in the stroma (17). Recently, Grosso *et al.* identified specific tumor immune microenvironment (TIME) metasignatures based on CD8+ infiltration and identified that fully inflamed tumors have elevated IFN, JAK/STAT and NFκB signatures (49). Additionally, the stroma of these tumors has higher levels of IFITM1 expression and low levels of MHC-class I molecules and elevated levels of PD-L1. Supporting this study, we have identified that loss of IFITM1 increases gene expression of HLA molecules (HLA-A,B,C,E,F) and decreases PD-L1 expression (data not shown), suggesting a rationale for the investigation of the role of IFITM1 in immune checkpoint regulation.

IFITM1 can be regulated by IFNα signaling and by NFκB (16, 23). Our data supports JAK/STAT involvement in driving IFITM1 expression in TNBC, but evidence presented herein also suggest an alternative mechanism involving IFNα and NFκB crosstalk. We show that inhibition of autocrine IFNα signaling and loss of STAT2 and IRF9 significantly reduces IFITM1 expression; however, loss of p65 and use of the NFκB inhibitor, parthenolide, significantly reduce IFITM1 expression as well. Previous studies highlight IFITM1 as a non-canonical ISG since it can be regulated independently of the phosphorylated-ISGF3 complex (50). STAT proteins in their unphosphorylated form and the NFκB signaling molecule, p65,

have a coordinated effort in driving ISG expression. This is evidenced by p65 being required for ISG induction in the absence of pSTATs and p65 dependence on unphosphorylated-STAT2 (U-STAT2) for nuclear translocation (51, 52). Notably, the TNBC cells used in this study have very low levels of pSTAT2 on basal level and we have previously shown that the deletion of the region containing the NFκB element in the IFITM1 promoter significantly diminishes promoter activity (14). Perhaps this could be attributed to the recently discovered phenomenon that U-STAT2 can bridge DNA bound p65 and IRF9 to induce full transriptional activation of specific genes (52) since p65 can directly bind to the promoter of IFITM1 (23). Supporting this evidence, investigation using the depmap.com portal suggest correlation of IFNα and IFITM1 in MDA-MB-157 and MDA-MB-468 cell lines (data not shown). Alternatively, the crosstalk between NFκB and IFNα may hinge on IKKα. IKKα is a regulator of NFκB signaling that can induce IRF7 driven IFN activation and subsequent NFκB signaling independent of IκB disassociation resulting in a positive IFN feedback loop (18). Alternative pathways of ISG induction have likely evolved to control infection upon inhibition of canonical JAK/STAT signaling to minimize the risk of aberrant signaling and infection; however, our evidence suggests that alternative IFN signaling play a role in cancer progression through crosstalk with NFκB and subsequent induction of IFITM1.

High-throughput drug cytotoxicity screening is a method used for rapid identification of FDA-approved and abandoned drugs which have the potential to be repurposed outside of the scope of the original proposed application (53). Our high throughput screen identified parthenolide, a sesquiterpene lactone derived from the feverfew plant, and a known NFκB inhibitor, as a potent growth inhibitor of TNBC cells with the ability to suppress IFITM1 expression. Prior to our study, parthenolide was tested using MDA-MB-231 cells where it was shown to promote cell death, inhibit metastasis, and decrease *in vivo* growth (54–56). Similarly, we show that parthenolide significantly reduces tumor growth and increases apoptosis in MDA-MB-468 and SUM149 cells which is associated with a decrease in phospho-p65 and IFITM1 expression. Notably, the inhibitory effect of parthenolide on IFITM1 and phospho-p65 *in vivo* was less pronounced than its effect on these proteins *in vitro*, thus highlighting the importance of the tumor microenvironment in impacting the efficacy of parthenolide *in vivo*. Also, altered metabolism of parthenolide *in vivo* (57, 58) may impact its efficacy thus requiring a higher dose of the drug to produce similar effects to those seen *in vitro*.

An interesting finding is that MDA-MB-231 cells, which lack IFITM1, have a significantly higher IC50 of parthenolide compared SUM149, MDA-MB-157 and MDA-MB-468 TNBC cells which all express IFITM1 (Supplemental Table 1), suggesting that the presence of IFITM1 might sensitize TNBC cells to parthenolide. This assertion, however, is contradicted by our observation that knockout of IFITM1 in SUM149 and MDA-MB-157 cells enhances their sensitivity to parthenolide, suggesting that parthenolide does not directly target IFITM1 but rather targets NFκB to suppress IFITM1. Supporting this evidence, IFITM1 has been identified as an ISG involved in the interferon related DNA damage response signature, suggesting that IFITM1 may function as an important mediator of the cell response to external stressors including drug treatment (11). Though this specific phenomenon was not examined *in vivo*, future studies are essential to confirm how the loss of IFITM1 alters TNBC response to specific treatment strategies. Lastly, aside from NFκB inhibition, it is

important to note that parthenolide has been shown to have multiple targets in tumor cells including: binding directly to focal adhesion kinase in MDA-MB-231 breast cancer cells when treated with high doses (56), increasing autophagy, generating reactive oxygen species, activating of JNK, or inhibiting the JAK2-STAT3 axis (54, 55, 59, 60); though each of these pathways can regulate NFκB.

Tumor acquired drug resistance and off target effects of cancer drugs are essential determinants of drug efficacy. Approximately 70% of TNBC patients do not respond to conventional chemotherapy (8) and elevated IFN signature, including IFITM1 overexpression, contributes to drug and radiation resistance in breast cancer (11). Regarding parthenolide, studies have reported that it has the ability to synergize and cooperate with anti-cancer agents in multiple malignancies including breast cancer (60). Use of MDA-MB-231 cells shows a synergistic effect of parthenolide with docetaxel, paclitaxel, doxorubicin, SAHA, TRAIL, and vinorelbine while use of parthenolide in MCF-7 cells has a synergistic effect with 4-hydroxytamoxifen, tamoxifen, and fulvestrant. Though parthenolide represents an opportunity to further validate IFITM1 as a promising drug target for TNBC, future studies investigating resistance mechanisms and combination therapies are essential. Specifically, it will be important to investigate how long-term treatment with parthenolide alters JAK/STAT signaling due to the proposed mechanistic crosstalk between NFκB and IFN signaling. Lastly, parthenolide is highly lipophilic which limits its bioavailability, however, derivatives with improved solubility have been developed such as dimethylaminoparthenolide, which could eventually be used in patient populations (54, 61).

Collectively, evidence presented herein demonstrate that either direct inhibition of IFITM1 or targeting its expression through interrupting IFNα/NFκB crosstalk with parthenolide, substantially attenuates TNBC tumor growth and migration. Parthenolide has historically been used for its anti-inflammatory and anti-migraine effects but is potentially beneficial for patients with TNBC (60). We acknowledge that IFNα/NFκB crosstalk has been introduced in previous studies (18, 19, 62), however, our findings suggest that both pathways play a critical role in regulating IFITM1 expression in TNBC cells thus providing additional insight into the pathogenesis of and therapeutic options for IFITM1 positive TNBC diagnoses.

Supplementary Material

Refer to Web version on PubMed Central for supplementary material.

Acknowledgments

FINANCIAL SUPPORT

This research was supported, in part, by grants from the National Institutes of Health-National Cancer Institute (K01CA120051 and 1F30CA203160-01), the Department of Defense (W81XWH-12-1-0139), the American Cancer Society (IRG-09-062-06), and the University of Kansas School of Medicine Investigator Assistance Award. The NCI-supported University of Kansas Cancer Center Support Grant (CCSG, P30CA168524-0) and the KUMC Biomedical Research Training Program (BRTP) also provided pilot funds to support this work. Additionally, funding provided by the Geographic Management of Cancer Health Disparities Program (GMaP) Region 3, a Supplement of the National Institutes of Health grant P30 CA118100 (Willman, CL) also supported this work. The content is solely the responsibility of the authors and does not necessarily represent the official views of the National Institutes of Health. Biospecimen and high throughput screening resources were provided by the Biospecimen Shared Resource (BSR) and Lead Development and Optimization Shared Resource (LDOSR), also

supported by the University of Kansas Cancer Center Support Grant. We acknowledge the Kansas Intellectual and Developmental Disabilities Research Center (KIDDRC) at the University of Kansas Medical Center, which is sponsored, in part, by the NIH cooperative agreement grant, U54 HD09216. We further acknowledge the Confocal Imaging Core at the University of Kansas Medical Center, which is supported in part, by NIH/NIGMS COBRE grant P30GM122731. The Leica STED microscope is supported by NIH1S10OD023625.

Abbreviations

AKT	Protein kinase B
ERK	Extracellular-signal-regulated kinase
CAV1	Caveolin-1
CD81	Cluster of differentiation 81
EGFR	Epidermal growth factor receptor
ER	Estrogen Receptor
ERα	Estrogen receptor alpha
HER2	Human epidermal growth factor receptor
IC50	Half maximal inhibitory concentration
IFITM1	Interferon induced transmembrane protein-1
IFNAR	Interferon alpha receptor
IFNAR nAb	Interferon alpha receptor neutralizing antibody
IFN	Interferon
IFNα	Interferon alpha
IL6	Interleukin-6
IPA	Ingenuity pathway analysis
IRF9	Interferon regulatory factor-9
ISGs	Interferon stimulated genes
ISGF3	Interferon stimulated gene factor-3
ISRE	Interferon stimulated response element
JAK	Janus activated kinase
NFκB	Nuclear factor kappa B
MIND	Mammary intraductal model
P65	NFκB p65 subunit
PI3K	Phosphoinositide 3-kinase

PN	Parthenolide
PR	Progesterone Receptor
SNAI2	Snail family transcriptional repressor-2
STAT1/2	Signal transducer and activator of transcription 1 and 2
TNBC	Triple-negative breast cancer
TYK	Tyrosine kinase

REFERENCES

1. Lehmann BD, Bauer JA, Chen X, Sanders ME, Chakravarthy AB, Shyr Y, et al. Identification of human triple-negative breast cancer subtypes and preclinical models for selection of targeted therapies. The Journal of clinical investigation. 2011;121(7):2750–67. [PubMed: 21633166]
2. Denkert C, Liedtke C, Tutt A, von Minckwitz G. Molecular alterations in triple-negative breast cancer-the road to new treatment strategies. Lancet. 2017;389(10087):2430–42. [PubMed: 27939063]
3. Cejalvo JM, Martinez de Duenas E, Galvan P, Garcia-Recio S, Burgues Gasion O, Pare L, et al. Intrinsic Subtypes and Gene Expression Profiles in Primary and Metastatic Breast Cancer. Cancer research. 2017;77(9):2213–21. [PubMed: 28249905]
4. Foulkes WD, Smith IE, Reis-Filho JS. Triple-negative breast cancer. The New England journal of medicine. 2010;363(20):1938–48. [PubMed: 21067385]
5. Prado-Vazquez G, Gamez-Pozo A, Trilla-Fuertes L, Arevalillo JM, Zapater-Moros A, Ferrer-Gomez M, et al. A novel approach to triple-negative breast cancer molecular classification reveals a luminal immune-positive subgroup with good prognoses. Scientific reports. 2019;9(1):1538. [PubMed: 30733547]
6. Ismail-Khan R, Bui MM. A review of triple-negative breast cancer. Cancer Control. 2010;17(3):173–6. [PubMed: 20664514]
7. Li X, Yang J, Peng L, Sahin AA, Huo L, Ward KC, et al. Triple-negative breast cancer has worse overall survival and cause-specific survival than non-triple-negative breast cancer. Breast cancer research and treatment. 2017;161(2):279–87. [PubMed: 27888421]
8. Cortazar P, Zhang L, Untch M, Mehta K, Costantino JP, Wolmark N, et al. Pathological complete response and long-term clinical benefit in breast cancer: the CTNeoBC pooled analysis. Lancet. 2014;384(9938):164–72. [PubMed: 24529560]
9. Buess M, Nuyten DS, Hastie T, Nielsen T, Pesich R, Brown PO. Characterization of heterotypic interaction effects in vitro to deconvolute global gene expression profiles in cancer. Genome biology. 2007;8(9):R191. [PubMed: 17868458]
10. Khodarev NN, Roizman B, Weichselbaum RR. Molecular pathways: interferon/stat1 pathway: role in the tumor resistance to genotoxic stress and aggressive growth. Clinical cancer research : an official journal of the American Association for Cancer Research. 2012;18(11):3015–21. [PubMed: 22615451]
11. Weichselbaum RR, Ishwaran H, Yoon T, Nuyten DS, Baker SW, Khodarev N, et al. An interferon-related gene signature for DNA damage resistance is a predictive marker for chemotherapy and radiation for breast cancer. Proceedings of the National Academy of Sciences of the United States of America. 2008;105(47):18490–5. [PubMed: 19001271]
12. Theofilopoulos AN, Baccala R, Beutler B, Kono DH. Type I interferons (alpha/beta) in immunity and autoimmunity. Annual review of immunology. 2005;23:307–36.
13. Lui AJ, Geanes ES, Ogony J, Behbod F, Marquess J, Valdez K, et al. IFITM1 suppression blocks proliferation and invasion of aromatase inhibitor-resistant breast cancer in vivo by JAK/STAT-mediated induction of p21. Cancer letters. 2017;399:29–43. [PubMed: 28411130]

14. Ogony J, Choi HJ, Lui A, Cristofanilli M, Lewis-Wambi J. Interferon-induced transmembrane protein 1 (IFITM1) overexpression enhances the aggressive phenotype of SUM149 inflammatory breast cancer cells in a signal transducer and activator of transcription 2 (STAT2)-dependent manner. Breast cancer research : BCR. 2016;18(1):25. [PubMed: 26897526]
15. Bertucci F, Finetti P, Vermeulen P, Van Dam P, Dirix L, Birnbaum D, et al. Genomic profiling of inflammatory breast cancer: a review. Breast (Edinburgh, Scotland). 2014;23(5):538–45.
16. Cheon H, Holvey-Bates EG, Schoggins JW, Forster S, Hertzog P, Imanaka N, et al. IFNbeta-dependent increases in STAT1, STAT2, and IRF9 mediate resistance to viruses and DNA damage. The EMBO journal. 2013;32(20):2751–63. [PubMed: 24065129]
17. Provance OK, Lewis-Wambi J. Deciphering the role of interferon alpha signaling and microenvironment crosstalk in inflammatory breast cancer. Breast cancer research : BCR. 2019;21(1):59. [PubMed: 31060575]
18. Pfeffer LM. The role of nuclear factor kappaB in the interferon response. J Interferon Cytokine Res. 2011;31(7):553–9. [PubMed: 21631354]
19. Yang CH, Murti A, Pfeffer SR, Kim JG, Donner DB, Pfeffer LM. Interferon alpha /beta promotes cell survival by activating nuclear factor kappa B through phosphatidylinositol 3-kinase and Akt. J Biol Chem. 2001;276(17):13756–61. [PubMed: 11278812]
20. Wienerroither S, Shukla P, Farlik M, Majoros A, Stych B, Vogl C, et al. Cooperative Transcriptional Activation of Antimicrobial Genes by STAT and NF-kappaB Pathways by Concerted Recruitment of the Mediator Complex. Cell Rep. 2015;12(2):300–12. [PubMed: 26146080]
21. Iwanaszko M, Kimmel M. NF-κB and IRF pathways: cross-regulation on target genes promoter level. BMC Genomics. 2015;16(1):307. [PubMed: 25888367]
22. Csumita M, Csermely A, Horvath A, Nagy G, Monori F, Göczi L, et al. Specific enhancer selection by IRF3, IRF5 and IRF9 is determined by ISRE half-sites, 5' and 3' flanking bases, collaborating transcription factors and the chromatin environment in a combinatorial fashion. Nucleic Acids Res. 2020;48(2):589–604. [PubMed: 31799619]
23. Kim SH, In Choi H, Choi MR, An GY, Binas B, Jung KH, et al. Epigenetic regulation of IFITM1 expression in lipopolysaccharide-stimulated human mesenchymal stromal cells. Stem Cell Res Ther. 2020;11(1):16. [PubMed: 31910882]
24. Wilkins C, Woodward J, Lau DT, Barnes A, Joyce M, McFarlane N, et al. IFITM1 is a tight junction protein that inhibits hepatitis C virus entry. Hepatology. 2013;57(2):461–9. [PubMed: 22996292]
25. Hatano H, Kudo Y, Ogawa I, Tsunematsu T, Kikuchi A, Abiko Y, et al. IFN-induced transmembrane protein 1 promotes invasion at early stage of head and neck cancer progression. Clinical cancer research : an official journal of the American Association for Cancer Research. 2008;14(19):6097–105. [PubMed: 18829488]
26. Lee J, Goh SH, Song N, Hwang JA, Nam S, Choi IJ, et al. Overexpression of IFITM1 has clinicopathologic effects on gastric cancer and is regulated by an epigenetic mechanism. The American journal of pathology. 2012;181(1):43–52. [PubMed: 22609115]
27. Yu F, Xie D, Ng SS, Lum CT, Cai MY, Cheung WK, et al. IFITM1 promotes the metastasis of human colorectal cancer via CAV-1. Cancer letters. 2015;368(1):135–43. [PubMed: 26259513]
28. Escher TE, Lui AJ, Geanes ES, Walter KR, Tawfik O, Hagan CR, et al. Interaction Between MUC1 and STAT1 Drives IFITM1 Overexpression in Aromatase Inhibitor-Resistant Breast Cancer Cells and Mediates Estrogen-Induced Apoptosis. Mol Cancer Res. 2019;17(5):1180–94. [PubMed: 30655323]
29. Xu YY, Yu HR, Sun JY, Zhao Z, Li S, Zhang XF, et al. Upregulation of PITX2 Promotes Letrozole Resistance Via Transcriptional Activation of IFITM1 Signaling in Breast Cancer Cells. Cancer Res Treat. 2019;51(2):576–92. [PubMed: 30025446]
30. Yang J, Li L, Xi Y, Sun R, Wang H, Ren Y, et al. Combination of IFITM1 knockdown and radiotherapy inhibits the growth of oral cancer. Cancer science. 2018;109(10):3115–28. [PubMed: 29770536]

31. Kim NH, Sung HY, Choi EN, Lyu D, Choi HJ, Ju W, et al. Aberrant DNA methylation in the IFITM1 promoter enhances the metastatic phenotype in an intraperitoneal xenograft model of human ovarian cancer. Oncology reports. 2014;31(5):2139–46. [PubMed: 24676393]
32. Sari IN, Yang YG, Phi LT, Kim H, Baek MJ, Jeong D, et al. Interferon-induced transmembrane protein 1 (IFITM1) is required for the progression of colorectal cancer. Oncotarget. 2016;7(52):86039–50. [PubMed: 27852071]
33. Yang YG, Koh YW, Sari IN, Jun N, Lee S, Phi LTH, et al. Interferon-induced transmembrane protein 1-mediated EGFR/SOX2 signaling axis is essential for progression of non-small cell lung cancer. International journal of cancer. 2018.
34. Lewis JS, Meeke K, Osipo C, Ross EA, Kidawi N, Li T, et al. Intrinsic mechanism of estradiol-induced apoptosis in breast cancer cells resistant to estrogen deprivation. J Natl Cancer Inst. 2005;97(23):1746–59. [PubMed: 16333030]
35. Behbod F, Kittrell FS, LaMarca H, Edwards D, Kerbawy S, Heestand JC, et al. An intraductal human-in-mouse transplantation model mimics the subtypes of ductal carcinoma in situ. Breast cancer research : BCR. 2009;11(5):R66. [PubMed: 19735549]
36. Andrews S FastQC: a quality control tool for high throughput sequence data. Available online at: http://www.bioinformatics.babraham.ac.uk/projects/fastqc. 2010.
37. Benjamini Y, Hochberg Y. Controlling the false discovery rate: a practical and powerful approach to multiple testing. Journal of the Royal Statistical Society Series B (Methodological). 1995:289–300.
38. Chandrashekar DS, Bashel B, Balasubramanya SAH, Creighton CJ, Ponce-Rodriguez I, Chakravarthi B, et al. UALCAN: A Portal for Facilitating Tumor Subgroup Gene Expression and Survival Analyses. Neoplasia. 2017;19(8):649–58. [PubMed: 28732212]
39. Győrffy B, Lanczky A, Eklund AC, Denkert C, Budczies J, Li Q, et al. An online survival analysis tool to rapidly assess the effect of 22,277 genes on breast cancer prognosis using microarray data of 1,809 patients. Breast Cancer Res Treat. 2010;123(3):725–31. [PubMed: 20020197]
40. Rhodes DR, Kalyana-Sundaram S, Mahavisno V, Varambally R, Yu J, Briggs BB, et al. Oncomine 3.0: genes, pathways, and networks in a collection of 18,000 cancer gene expression profiles. Neoplasia. 2007;9(2):166–80. [PubMed: 17356713]
41. Rhodes DR, Yu J, Shanker K, Deshpande N, Varambally R, Ghosh D, et al. ONCOMINE: a cancer microarray database and integrated data-mining platform. Neoplasia. 2004;6(1):1–6. [PubMed: 15068665]
42. Jezequel P, Campone M, Gouraud W, Guerin-Charbonnel C, Leux C, Ricolleau G, et al. bc-GenExMiner: an easy-to-use online platform for gene prognostic analyses in breast cancer. Breast Cancer Res Treat. 2012;131(3):765–75. [PubMed: 21452023]
43. Wang M, Zhang Y, Xu Z, Qian P, Sun W, Wang X, et al. RelB sustains endocrine resistant malignancy: an insight of noncanonical NF-κB pathway into breast Cancer progression. Cell Commun Signal. 2020;18(1):128. [PubMed: 32807176]
44. Sovak MA, Bellas RE, Kim DW, Zanieski GJ, Rogers AE, Traish AM, et al. Aberrant nuclear factor-kappaB/Rel expression and the pathogenesis of breast cancer. The Journal of clinical investigation. 1997;100(12):2952–60. [PubMed: 9399940]
45. Vences-Catalan F, Duault C, Kuo CC, Rajapaksa R, Levy R, Levy S. CD81 as a tumor target. Biochem Soc Trans. 2017;45(2):531–5. [PubMed: 28408492]
46. Wright MD, Moseley GW, van Spriel AB. Tetraspanin microdomains in immune cell signalling and malignant disease. Tissue Antigens. 2004;64(5):533–42. [PubMed: 15496196]
47. Siegrist F, Ebeling M, Certa U. The small interferon-induced transmembrane genes and proteins. Journal of interferon & cytokine research : the official journal of the International Society for Interferon and Cytokine Research. 2011;31(1):183–97.
48. Kim JY, Kim H, Suk K, Lee WH. Activation of CD147 with cyclophilin a induces the expression of IFITM1 through ERK and PI3K in THP-1 cells. Mediators of inflammation. 2010;2010:821940. [PubMed: 20847954]
49. Gruosso T, Gigoux M, Manem VSK, Bertos N, Zuo D, Perlitch I, et al. Spatially distinct tumor immune microenvironments stratify triple-negative breast cancers. The Journal of clinical investigation. 2019;129(4):1785–800. [PubMed: 30753167]

50. Rong L, Li R, Li S, Luo R. Immunosuppression of breast cancer cells mediated by transforming growth factor-beta in exosomes from cancer cells. Oncology letters. 2016;11(1):500–4. [PubMed: 26870240]
51. Alazawi W, Heath H, Waters JA, Woodfin A, O'Brien AJ, Scarzello AJ, et al. Stat2 loss leads to cytokine-independent, cell-mediated lethality in LPS-induced sepsis. Proc Natl Acad Sci U S A. 2013;110(21):8656–61. [PubMed: 23653476]
52. Nan J, Wang Y, Yang J, Stark GR. IRF9 and unphosphorylated STAT2 cooperate with NF-kappaB to drive IL6 expression. Proc Natl Acad Sci U S A. 2018;115(15):3906–11. [PubMed: 29581268]
53. Pushpakom S, Iorio F, Eyers PA, Escott KJ, Hopper S, Wells A, et al. Drug repurposing: progress, challenges and recommendations. Nat Rev Drug Discov. 2019;18(1):41–58. [PubMed: 30310233]
54. D'Anneo A, Carlisi D, Lauricella M, Puleio R, Martinez R, Di Bella S, et al. Parthenolide generates reactive oxygen species and autophagy in MDA-MB231 cells. A soluble parthenolide analogue inhibits tumour growth and metastasis in a xenograft model of breast cancer. Cell death & disease. 2013;4:e891. [PubMed: 24176849]
55. Carlisi D, Buttitta G, Di Fiore R, Scerri C, Drago-Ferrante R, Vento R, et al. Parthenolide and DMAPT exert cytotoxic effects on breast cancer stem-like cells by inducing oxidative stress, mitochondrial dysfunction and necrosis. Cell death & disease. 2016;7:e2194. [PubMed: 27077810]
56. Berdan CA, Ho R, Lehtola HS, To M, Hu X, Huffman TR, et al. Parthenolide Covalently Targets and Inhibits Focal Adhesion Kinase in Breast Cancer Cells. Cell chemical biology. 2019.
57. Carlisi D, Buttitta G, Di Fiore R, Scerri C, Drago-Ferrante R, Vento R, et al. Parthenolide and DMAPT exert cytotoxic effects on breast cancer stem-like cells by inducing oxidative stress, mitochondrial dysfunction and necrosis. Cell death & disease. 2016;7(4):e2194. [PubMed: 27077810]
58. D'Anneo A, Carlisi D, Lauricella M, Puleio R, Martinez R, Di Bella S, et al. Parthenolide generates reactive oxygen species and autophagy in MDA-MB231 cells. A soluble parthenolide analogue inhibits tumour growth and metastasis in a xenograft model of breast cancer. Cell death & disease. 2013;4(10):e891. [PubMed: 24176849]
59. Liu M, Xiao C, Sun M, Tan M, Hu L, Yu Q. Parthenolide Inhibits STAT3 Signaling by Covalently Targeting Janus Kinases. Molecules. 2018;23(6).
60. Sztiller-Sikorska M, Czyz M. Parthenolide as Cooperating Agent for Anti-Cancer Treatment of Various Malignancies. Pharmaceuticals (Basel). 2020;13(8).
61. Freund RRA, Gobrecht P, Fischer D, Arndt HD. Advances in chemistry and bioactivity of parthenolide. Nat Prod Rep. 2020;37(4):541–65. [PubMed: 31763637]
62. Kwok BH, Koh B, Ndubuisi MI, Elofsson M, Crews CM. The anti-inflammatory natural product parthenolide from the medicinal herb Feverfew directly binds to and inhibits IkappaB kinase. Chemistry & biology. 2001;8(8):759–66. [PubMed: 11514225]

Highlights

1. Interferon induced transmembrane protein 1 (IFITM1) is overexpressed in a subset of TNBC tumors and is correlated with decreased relapse free survival
2. Loss of IFITM1 suppresses TNBC tumor growth and invasion *in vitro* and *in vivo* which is associated with changes in NFκB signaling
3. IFITM1 expression is regulated by crosstalk between IFNα and NFκB signaling
4. Parthenolide inhibits NFκB and IFNα crosstalk to mitigate IFITM1 expression and subsequent TNBC aggression

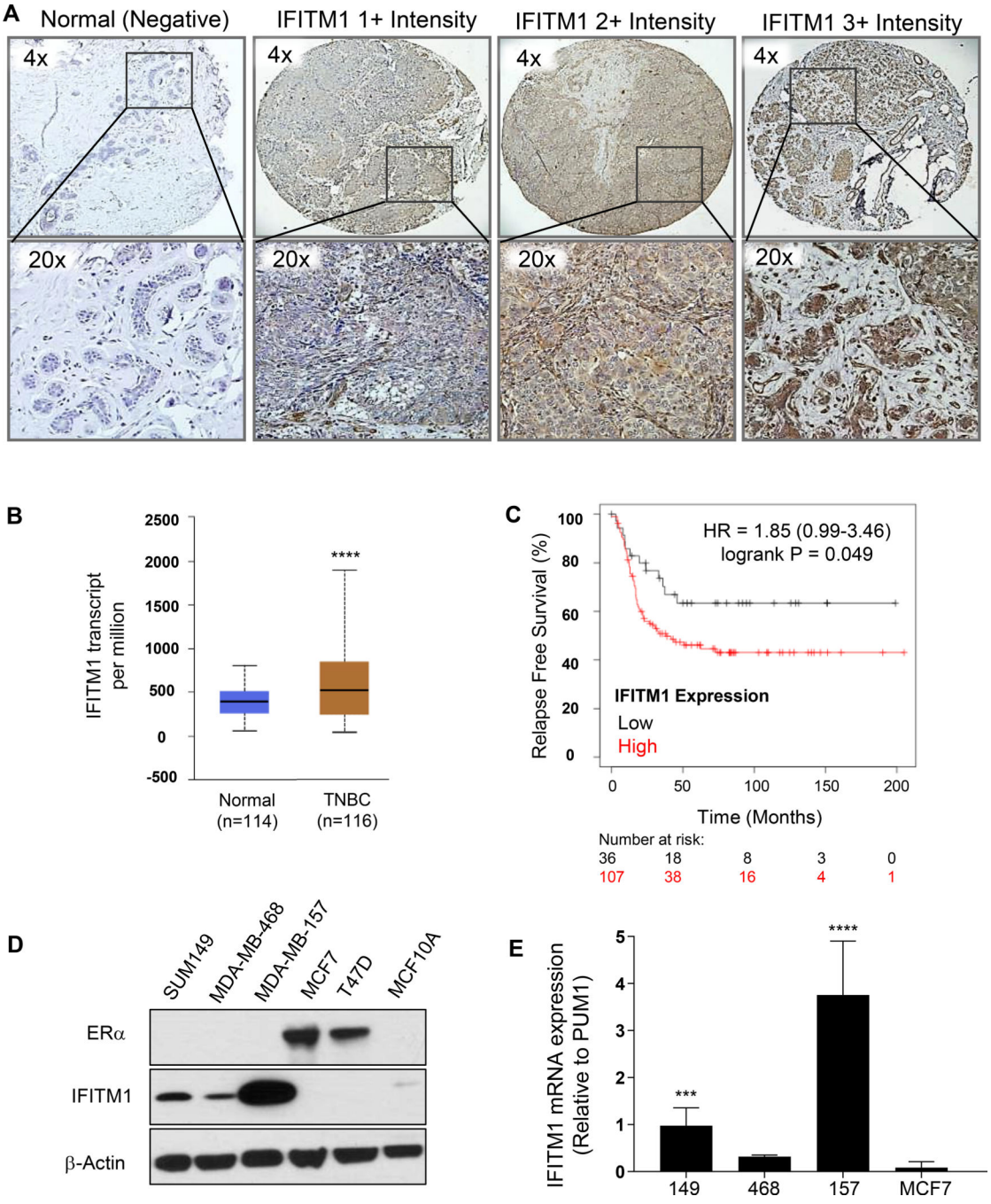

Figure 1: IFITM1 is overexpressed in triple-negative breast cancer.

A, Human TNBC breast tissue (34 samples) and normal tissue (6 samples) was obtained from the Biosample Repository at KUMC and stained for IFITM1 expression using immunohistochemistry. 62% had 1+ staining, 26% had 2+ staining and 12% had 3+ staining. **B,** The UALCAN database was used to assess IFITM1 expression in TCGA data. **C,** IFITM1 on relapse free survival derived from KM Plotter. Patients were first stratified into basal-like breast cancer and by the mesenchymal TNBC phenotype as defined by Pietenpol (1). **D,** Immunoblotting was used to assess IFITM1 protein expression in multiple TNBC

cell lines (SUM149, MDA-MB-468, MDA-MB-157), ER+ breast cancer cell lines (MCF7, T47D) and normal-immortalized human breast cells (MCF10A). **E,** IFITM1 mRNA expression measured by qRT-PCR in SUM149, MDA-MB-468, MDA-MB-157, and MCF-7 cell lines. Values represent means ± SD of three biological replicates and data are presented as fold change to PUM1 using the ΔCT method. Significance of expression compared to MCF-7 cells is represented.

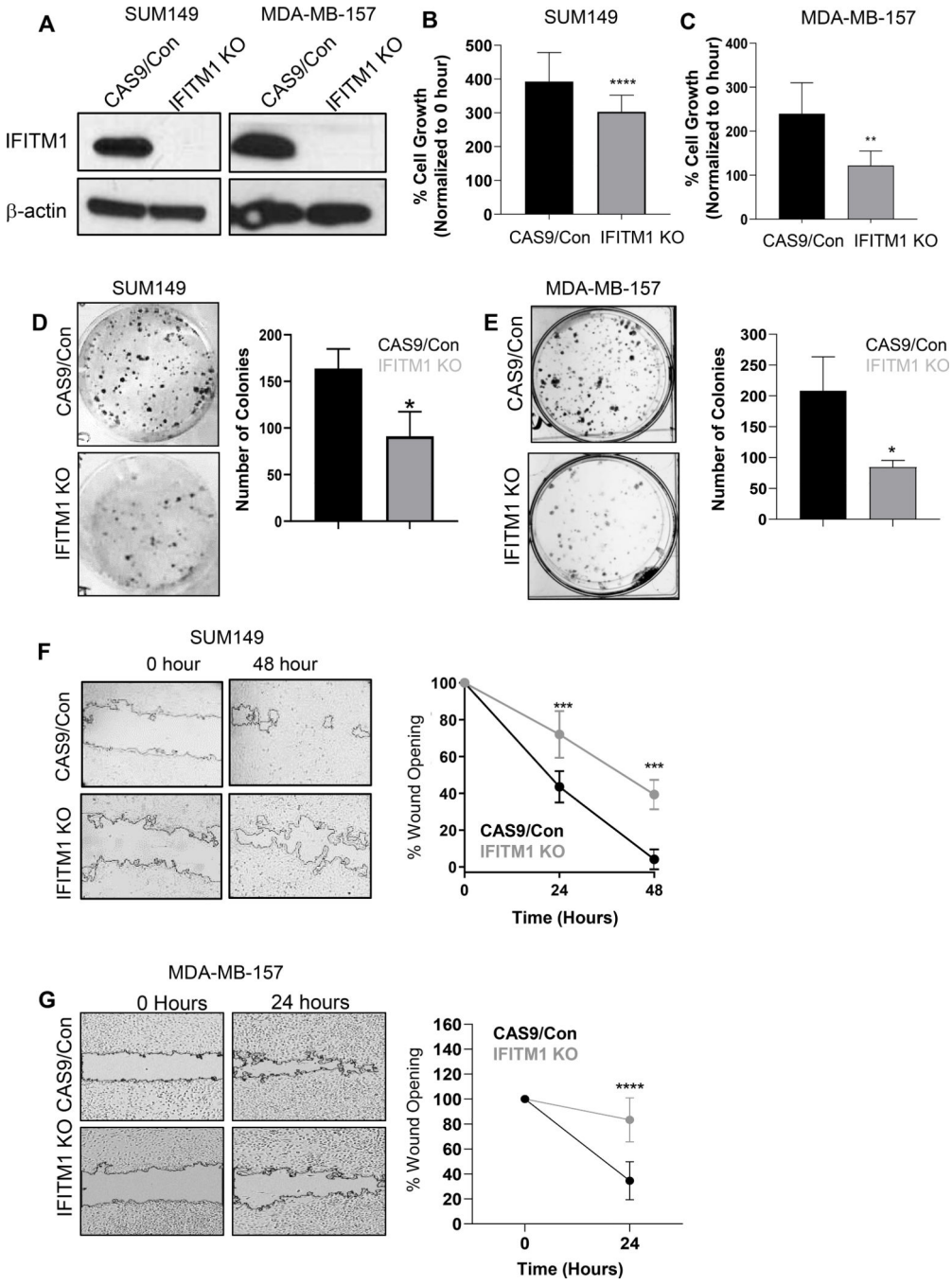

Figure 2: IFITM1 contributes to *in vitro* TNBC growth and migration.

A, Immunoblot of MDA-MB-157 and SUM149 cells depicting CRISPR/Cas9 knockout of IFITM1 expression **B-C,** MDA-MB-157 and SUM149 proliferation was measured through cell counting after 48 hours. Values represent means ± SD of at least three independent experiments done in triplicate. A t-test was used to assess statistical significance. **p<0.01, ***p<0.001 **D-E** The clonogenicity of SUM149 CAS9/Control and SUM149 IFITM1 KO cells (**D**) or MDA-MB-157 CAS9/Con and MDA-MB-157 IFITM1 KO cells (**E)** was assessed by plating 1,000 cells in a 6-well plate. After 10 days, cells were stained with

crystal violet and quantified based on colony number using ImageJ (right). Values represent means ± SD of three independent experiments conducted in duplicate. A t-test was used to assess statistical significance; *p<0.05. **F-G,** Scratch assay was conducted on 80% confluent plates of SUM149 CAS9/Control and SUM149 IFITM1 KO cells (**F**) or MDA-MB-157 CAS9/Con or MDA-MB-157 IFITM1 KO cells (**G**). Plates were imaged at 0, 24, and 48 hours and the size of the wound was quantified by ImageJ (right). Values represent means ± SD of four independent experiments conducted in quadruplicate. A t-test was used to assess statistical significance at each timepoint; ***p<0.001.

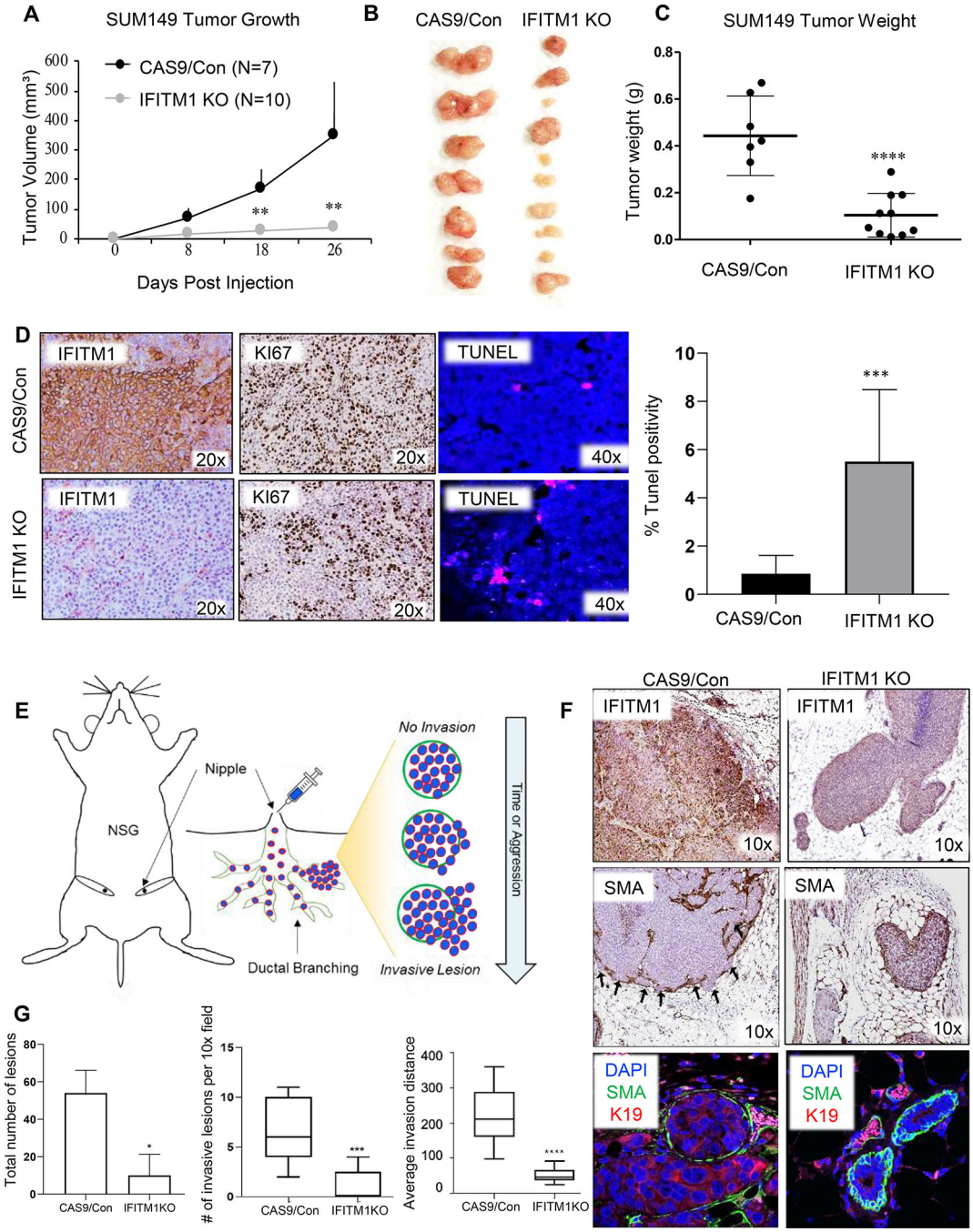

Figure 3: Loss of IFITM1 results in decreased growth and invasion *in vivo*.

A, 3 million SUM149 CAS9/Control or IFITM1 KO cells were injected bilaterally into the 4th mammary fat pad of female NSG mice. Tumor growth was measured over the course of 26 days and the difference of tumor volume between groups was assessed using a t-test at each time point **p<0.01 **B,** Images of the tumors derived from fat pad injections. **C,** Final tumor weight of CAS9/Control and IFITM1 KO tumors. Values represent means ± SD of 5 mice per group. Significance was assessed using a t-test ****p<0.0001. **D,** IHC analysis was used to assess IFITM1 and Ki67 expression and the Click-iT™ Plus TUNEL kit was used to

stain for apoptotic cells within the tumor. Quantification was completed using ImageJ software and a t-test was used to assess the significance of the percentage of cells with TUNEL staining ***p<0.001. **E,** Schematic of the mammary intraductal mouse model. **F,** Mammary glands were fixed and processed onto glass slides and H&E staining with IHC was used to assess tissue architecture and IFITM1 expression, while SMA was used to stain the milk duct. Immunofluorescent staining of the mammary glands (Bottom). Nuclei were stained with DAPI, milk ducts were stained with smooth muscle actin (SMA; green) and human keratin 19 (K19; red) stained the injected human epithelial breast cancer cells. **G,** Total number of lesions were quantified by counting the number of proliferative lesions in 3 tumors. Number of invasive lesions were quantified in each 10x field when clear invasion into the stroma with degradation of SMA was visible. Average invasion distance was quantified by measuring distance of K19 staining from SMA in immunofluorescent images using ImageJ. Data represented are from a single experiment.

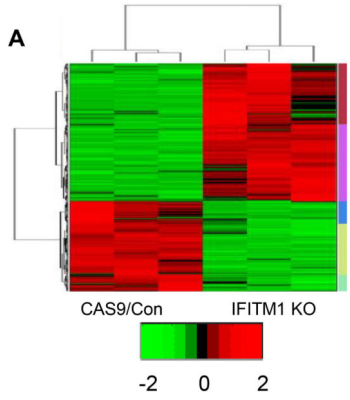

B

Downregulated in IFITM1 KO			
Pathway	**P-Value**	**Gene #**	**Z-score**
Proliferation of tumor cell lines	6.4E-13	78	-0.114
Migration of tumor cell lines	6.4E-6	37	-2.475
Invasion of tumor cell lines	8.4E-8	40	-2.1

C

Ingenuity Pathway Analysis			
Upstream Regulator	**Expr Fold Change**	**Activation z-score**	**p-value of overlap**
NFKB Complex		**-3.954**	**4.39E-13**
P65 (RELA)	-1.493	-3.854	9.31E-11
IkBα (NFKBIA)	-1.153	-2.890	7.10E-10
c-Rel (REL)	-1.001	-2.010	5.91E-6
p105 (NFKB1)	-1.429	-2.4475	2.41E-09
P100 (NFKB2)	-2.381	-1.727	5.49E-05

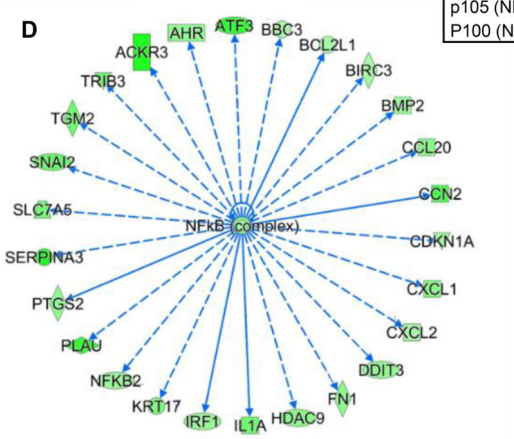

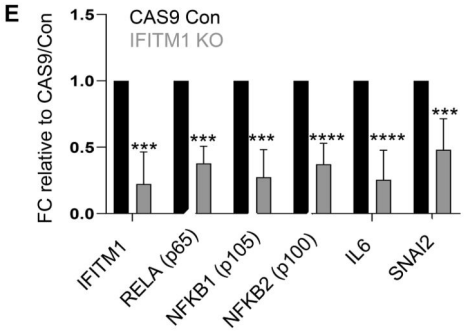

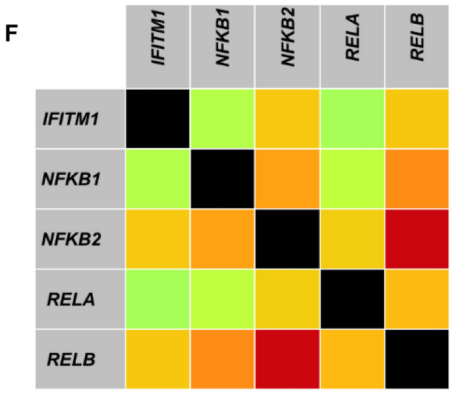

	RELA	RELB	NFKB1	NFKB2
IFITM1	R=0.13 P=0.01	R=0.37 P=<0.0001	R=0.16 P=0.054	R=0.37 <0.0001

Figure 4: Loss of IFITM1 decreases NFκB signaling and gene expression.

A, Heat map of the differentially expressed genes between CAS9/Control and IFITM1 KO cells showing upregulated (red) genes and downregulated (green) genes. **B,** Ingenuity pathway analysis (IPA) on the differentially expressed genes comparing IFITM1 KO to CAS9/Control. Negative Z-scores correlate to a decrease in pathway activation in IFITM1 KO cells. P-value and Z-score were computed within IPA. **C,** IPA upstream analysis summary **D,** IPA determined pathway of NFκB complex regulated genes with overlay of gene expression values of IFITM1 KO compared to CAS9/Control (dark green = >5 fold

downregulated). **E,** mRNA expression measured by qRT-PCR in SUM149 CAS9/Con and IFITM1 KO cell lines. Data represented as fold change compared to CAS9/Control via $2^{\wedge\Delta\Delta CT}$ method. Statistics were assessed on individual fold changes relative to PUM1 using a t-test with samples from three independent passages ***p<0.001, ****p<0.00001. **F,** The gene correlation targeted analysis on the BcGenExMiner platform was used to assess correlation between IFITM1 and NFκB elements. Search was performed using all available RNA-seq data (4,712 patients from TCGA, Brueffer et al. 2018 (Study code: GSE81538), and Saal et al. (Study code: GSE96058). R-values for Pearson's correlation values and p-values are listed below for IFITM1 and NFκB correlations.

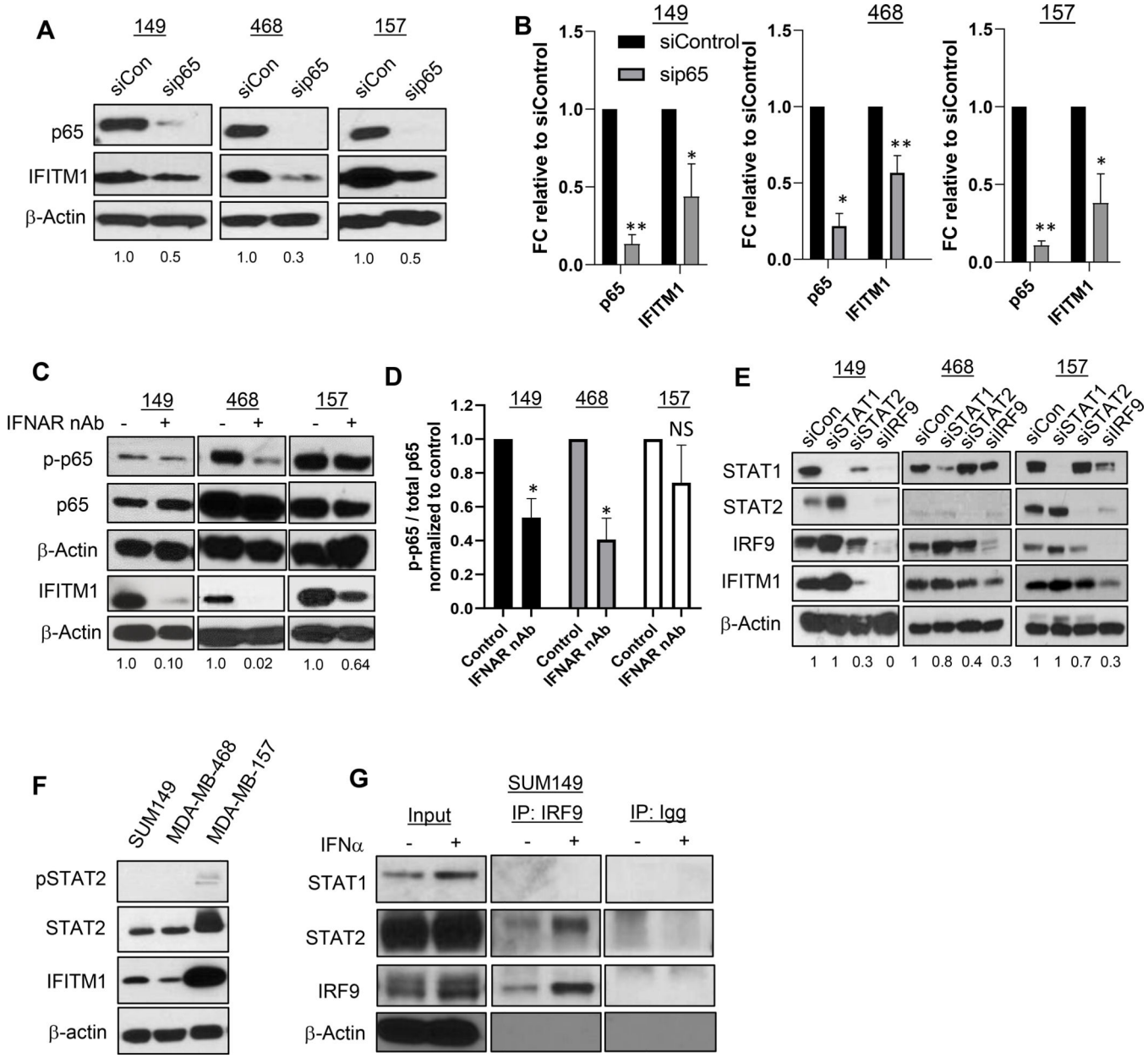

Figure 5: IFITM1 is regulated by NFκB and IFNα signaling in TNBC.

A, Immunoblotting assessed IFITM1 in multiple TNBC cell lines 48 hours after transfection with either siControl or sip65. Quantification of IFITM1 values are listed below. **B,** qRT-PCR assessed the gene expression of p65 and IFITM1 after transfection with either siControl or sip65. Data represented as fold change compared to siCon via $2^{\wedge\Delta\Delta CT}$ method. Values represent means ± SD of three independent experiments. Fold change relative to PUM1 was assessed with a t-test *p<0.05, **p<0.01, ***p<0.001. **C,** SUM149(149), MDA-MB-468 (468), and MDA-MB-157 (157) cells were treated with 5mM IFNAR2 neutralizing antibody for 24 hours and immunoblotted for p-p65 and IFITM1. Quantification of IFITM1 values are listed below and the ratio of p-p65/p65 is listed to the right (**D**). Values represent means ± SD of three independent experiments. A t-test was used to assess significance

*p<0.05. **E,** Immunoblotting was used to assess IFITM1 in multiple TNBC cell lines 48 hours after transfection with either siControl, siSTAT1, siSTAT2, or siIRF9. Quantification of IFITM1 values are listed below **F,** pSTAT2 expression was assessed in all TNBC cell lines **G,** Co-immunoprecipitation of STAT1 and STAT2 with IRF9 in SUM149 cells treated without or with 500 units/mL IFNα-2a for 2 hours.

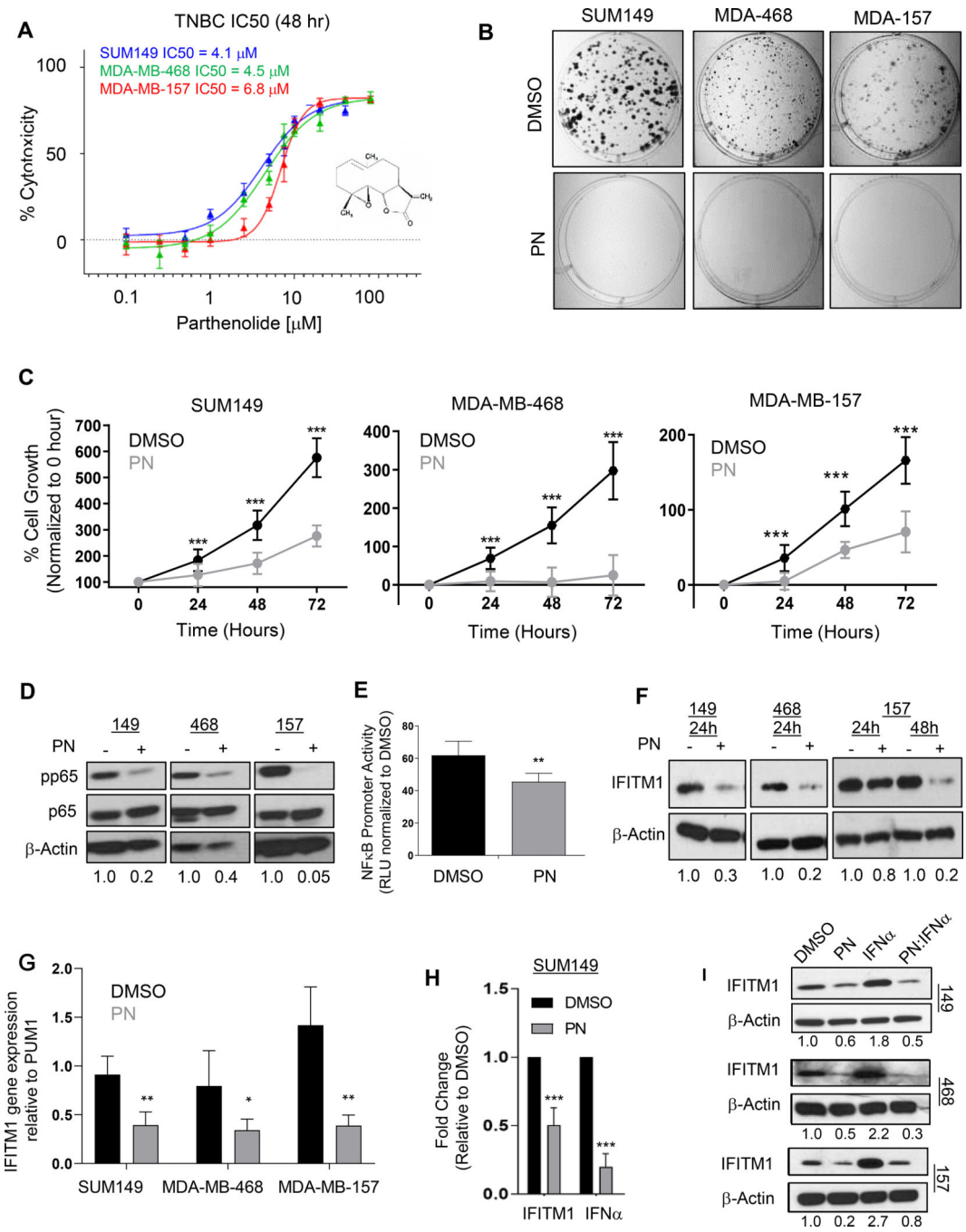

Figure 6: Using parthenolide to target IFNα and NFκB signaling inhibits IFITM1 expression in TNBC.

A, SUM149, MDA-MB-468, MDA-MB-157 cells were seeded onto a 96-well plate at 5,000 cells/well in 100μL. Twenty-four hours later, cells were treated with varying concentrations of parthenolide (PN) (0–80 μM) for 48 hours. After 48 hours, 10μL of 5 mg/mL 3-(4,5-dimethylthiazol-2-yl)-2,5-diphenyltetrazolium bromide (MTT) was added and incubated for 3 h at 37°C. The medium was then aspirated and 100μL of the solubilizing solution of a 1:1 solution of dimethyl sulfoxide and ethanol was added to dissolve blue formazan crystals.

Results were obtained by reading the plate at 570 nm. IC50 values were calculated by first normalizing each well to the average of the untreated wells which were then imported into GraphPad Prism version 5 for Windows (GraphPad Software, La Jolla, CA). The drug concentrations (X values) were transformed to a logarithmic scale while the Y values were transformed to percentages by multiplying these values by 100. To represent as percent cytotoxicity, Y values were further transformed using the equation, Y=K-Y. The IC50 and the 95% confidence interval were calculated by fitting the non-linear regression curve, log(inhibitor) vs. response – Variable slope (four parameters), to the data. **B,** Images of SUM149, MDA-MB-468 and MDA-MB-157 colony formation when treated with parthenolide at the IC50. Cells were treated every other day with the IC50 dose of parthenolide and grown for 10–14 days when colonies were stained with crystal violet and counted by ImageJ. **C,** SUM149, MDA-MB-468 and MDA-MB-157 breast cancer cells were treated with parthenolide at the IC50 and matched DMSO concentration followed by cell counting every 24 hours. The 0-hour time point represents cells counted prior to drug treatment. Values are normalized as percent growth from 0-hours. Values represent means ± SD of three independent experiments conducted in triplicate. A t-test was used to assess statistical significance at each timepoint; ***P<0.001 **D,** SUM149, MDA-MB-468 and MDA-MB-157 cells were treated for 24 hours with either parthenolide at the IC50 or with equal amount of DMSO followed by immunoblotting for phospho-p65 (S536) and total-p65 protein expression. Quantification of pp65/p65 ratios are listed below the blot. **E,** SUM149 cells were co-transfected with the DNA pGL4.32 NFκB-RE and Renilla constructs. Cells were treated with parthenolide at the IC50 or DMSO and luciferase was assayed 24 hours after treatment. Values represent means ± SD of four independent experiments conducted in triplicate. A t-test was used to assess statistical significance; **P<0.01. **F-G,** SUM149, MDA-MB-468 and MDA-MB-157 cells were treated with the parthenolide at the IC50 or with equal amount of DMSO for 24 followed by immunoblotting (quantification of IFITM1 values are listed below the blot) (**F**) or qRT-PCR (**G**) where data represents at least two independent experiments run in triplicate. A t-test was used to assess significance. *p<0.05, **p<0.01. **H,** IFITM1 and IFNα mRNA expression was assessed in SUM149 cells 24 hours after parthenolide or DMSO treatment by using qRT-PCR and is displayed as fold change relative to PUM1 using the equation 2^ΔCT. Data represents at least two independent experiments run in triplicate. A t-test was used to assess significance. ***p<0.001. **I,** SUM149, MDA-MB-468 and MDA-MB-157 cells were treated with DMSO, parthenolide at the IC50, 500 units/mL IFNα−2a or pre-treated for 4 hours with parthenolide at the IC50 followed by 20 hours treatment with 500 units/mL IFNα−2a. Samples were immunoblotted for IFITM1 expression and a representative blot with IFITM1 quantification is shown.

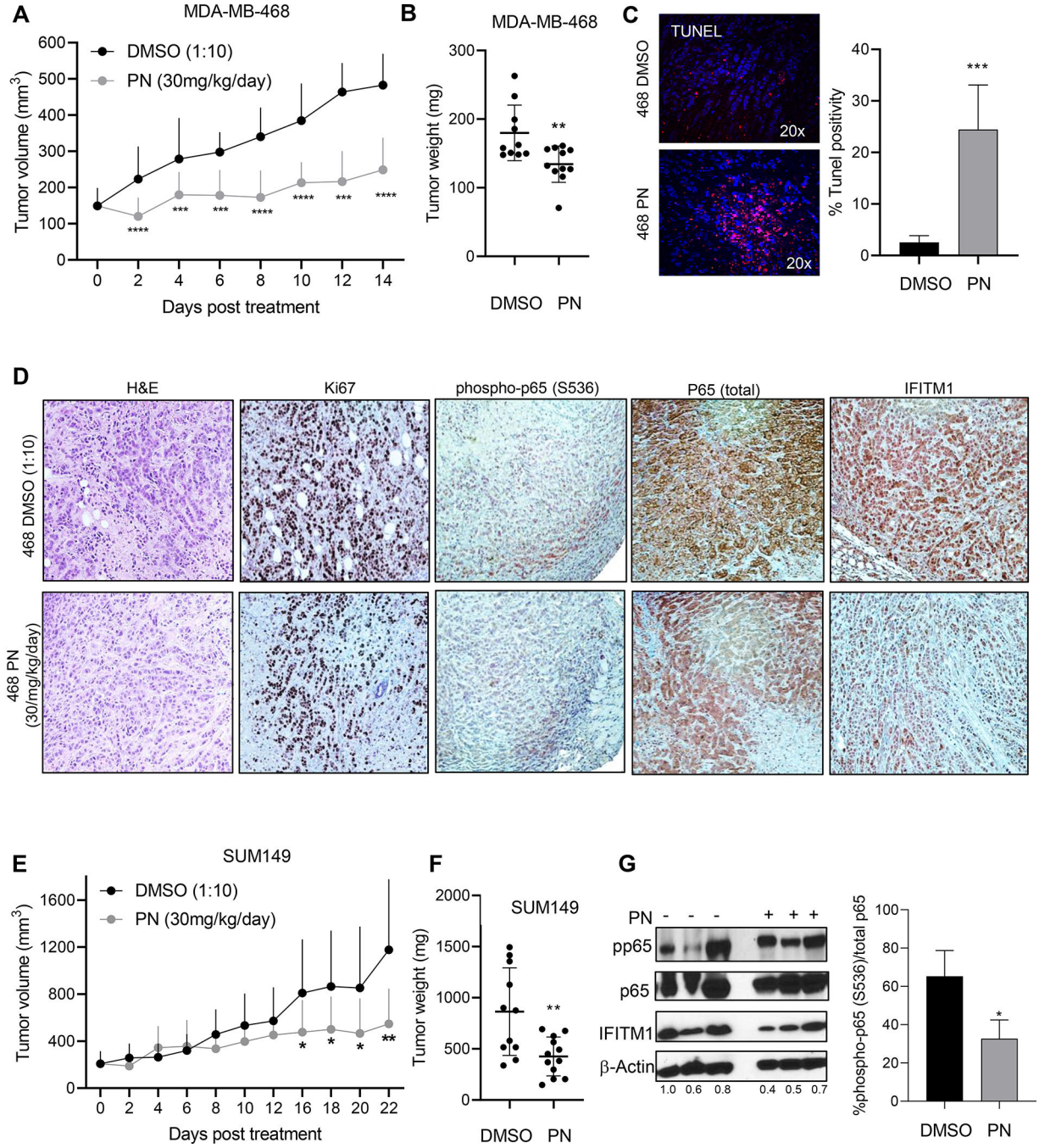

Figure 7: Parthenolide decrease TNBC tumor growth *in vivo*.

A, 3×10^6 MDA-MB-468 cells were injected bilaterally into the fat pad of 7-week old female NSG mice. Mice were treated with a 10% DMSO solution or 30mg/kg/day parthenolide for 14 days once tumors reached a mean volume of $150mm^3$. Tumors were measured every 48-hours and volume was calculated by $W^2/2L$. **B**, Final tumor weight of MDA-MB-468 DMSO and parthenolide treated tumors. **C,** The Click-iT™ Plus TUNEL kit was used to stain for apoptotic cells within the MDA-MB-468 tumor. Quantification (left) was completed using ImageJ software and a t-test was used to assess the significance of the

percentage of cells with TUNEL staining ***p<0.001. 0001. **D,** IHC analysis was used to assess phospho-and total p65, IFITM1 and Ki67 in DMSO and parthenolide treated MDA-MB-468 tumors. **C**, 3×106 SUM149 cells were injected bilaterally into the fat pad of 7-week old female NSG mice and the same MDA-MB-468 experimental design was followed. **F**, Final tumor weight after 21 days of either DMSO or parthenolide treatment in SUM149 cells. **F**, Western blot of three SUM149 DMSO treated tumors and four SUM149 parthenolide treated tumors. IFITM1 expression was quantified below and the ratio of phospho-p65 to p65 was quantified and plotted as a bar chart to assess significance (right).

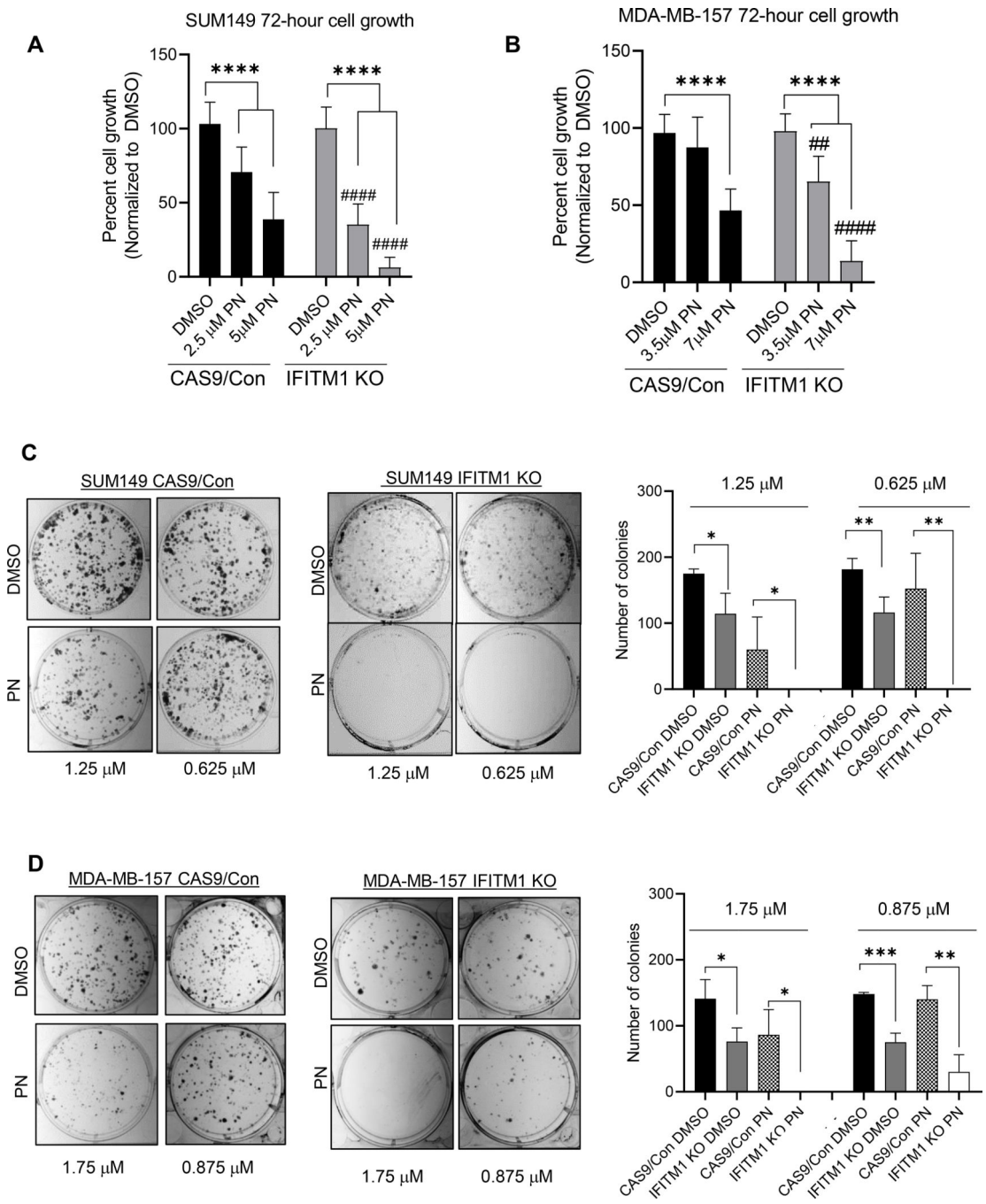

Figure 8: Loss of IFITM1 sensitizes SUM149 and MDA-MB-157 cells to parthenolide in vitro.

A, SUM149 and MDA-MB-157 (**B**) CAS9/Con and IFITM1 KO cells were treated with parthenolide at the IC50 and ½ IC50 followed by cell counting at 72-hours. Values are normalized to DMSO and represent means ± SD of four independent experiments conducted in triplicate. A t-test was used to assess statistical significance. Asterisks (*) represent significance within the specific clone assessed (CRISPR/Con or IFITM1 KO) while number signs (#) represent significance of the percent change between CRISPR/Con and IFITM1 KO cells.****p<0.0001, ####p<0.001, ## p<0.01. **C-D,** Images of SUM149 (**C**) and MDA-

MB-157 (**D**) CAS9/Con and IFITM1 KO colony formation when treated with fractionated doses of parthenolide. Cells were treated every other day with either 1/4 or 1/8 IC50 dose of parthenolide and grown for 10–14 days when colonies were stained with crystal violet and counted by ImageJ. Quantifications are to the right of the images. Values represent means ± SD of three independent experiments. *p<0.05, **p<0.01, ***p<0.005.

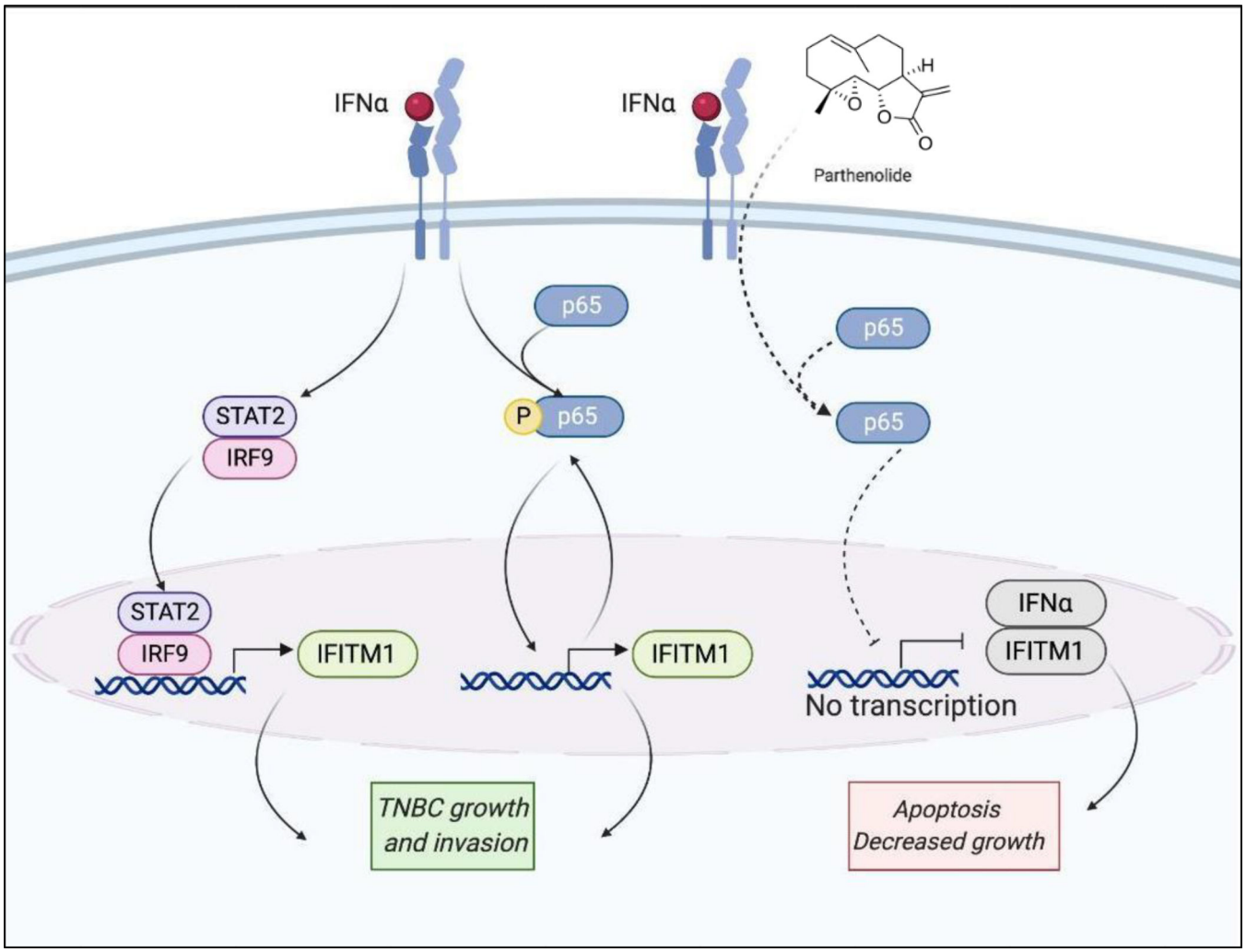

Figure 9: Schematic representation of IFNα and NFκB signaling regulating IFITM1 expression in TNBC.

Left, Non-canonical IFNα signaling through STAT2-IRF9 drives IFITM1 expression which promotes TNBC tumor growth and invasion. *Middle,* IFNα signaling contributes to a positive feedback loop activating p-p65 to promote IFITM1 expression. *Right*, Parthenolide targets p-p65/NFκB activation and inhibits IFNα signaling thus suppressing IFITM1 expression and inducing apoptosis and growth inhibition. Created with Biorender.com.

Table I.

Characteristics of patients included in the tissue microarray

	Frequency	Percent
Age		
25–35	5	15%
36–45	6	18%
46–55	6	18%
56–65	8	24%
66–75	6	18%
75+	3	9%
Race		
European American	26	76%
African American	6	18%
Asian/Pacific Islander	2	6%
Stage		
2	3	9%
3	31	91%
Her2/Neu Intensity		
0+	12	35.29%
0+	15	44.12%
1+	5	14.71%
2+	2	5.88%
Vascular invasion		
Present	7	21%
Absent	27	79%
Total	**34**	

Table II.

IFITM1 staining intensity in normal and TNBC breast tissues

Tissue Type	Intensity	Frequency	Percent
Normal Breast			
	0	6	100%
	1+	0	0%
	2+	0	0%
	3+	0	0%
	Total	**6**	
Breast Tumors			
	0	0	0%
	1+	21	62%
	2+	9	26%
	3+	4	12%
	Total	**34**	

Table III.

Primers sequences

Gene	Forward Primer (5'–3')	Reverse Primer (5'–3')
PUM1	TCACCGAGGCCCCTCTGAACCCTA	GGCAGTAATCTCCTTCTGCATCCT
IFITM1	GGATTTCGGCTTGTCCCGAG	CCATGTGGAAGGGAGGGCTC
IL6	CCTCCAGAACAGATTTGAGAGTAGT	GGGTCAGGGGTGGTTATTGC
IFNα-2a	CTTGAAGGACAGACATGACTTTGGA	GGATGGTTTCAGCCTTTTGGA
SNAI2	TGGTTGCTTCAAGGACACAT	GTTGCAGTGAGGGCAAGAA
RELA	AGCTCAAGATCTGCCGAGTG	ACATCAGCTTGCGAAAAGGA
NFKB1	GCAGCACTACTTCTTGACCACC	TCTGCTCCTGAGCATTGACGTC
NFKB2	GGCAGACCAGTGTCATTGAGCA	CAGCAGAAAGCTCACCACACTC